X-RAY PHOTON SPECTROSCOPY CALCULATIONS

Jorge E. Fernández* and Vincenzo G. Molinari

Laboratorio di Ingegneria Nucleare di Montecuccolino
University of Bologna
Via dei Colli 16, 40136 Bologna, Italy

I. INTRODUCTION

X-ray photons - as many other particles - interact with matter producing secondary radiation that carries useful information about the atoms comprising the target. The availability of intense sources of highly monochromatic X-rays and the great improvement in detector technology intensified research in X-ray spectrometry in the last twenty years. New techniques allowed the attenuation coefficients and the physics of the atom to be better known: Extended X-ray Absorption Fine Structure (EXAFS), X-ray Absorption Near Edge Structure (XANES), and Inelastic X-ray Scattering Spectroscopy (IXSS). Old techniques, like X-ray Fluorescence (XRF), gained in precision thus extending the horizon of applicability to new elements and energy ranges, and consequently Energy Dispersive X-ray Fluorescence (EDXRF) and Synchrotron Radiation X-ray Fluorescence (SRXRF) were evolved. Particle induced X-ray emission spectroscopy also benefited from this improvement. The field of application of X-ray spectrometry has grown from atomic, to nuclear, to plasma physics, to astrophysics.

Since X-rays are very penetrating they probe the depth of the target, sampling the information in an important volume. This makes it very probable that the secondary radiation may suffer further interactions with other atoms before leaving the specimen. Under these conditions, a multiple scattering scheme within transport theory seems to be the simplest approach to study the diffusion of X-rays adequately in a dense material.

---

* On leave of absence from the Faculty of Mathematics, Astronomy and Physics (FaMAF), University of Córdoba, Argentina. Fellow of CONICET, Buenos Aires, Argentina.

Advances in Nuclear Science and Technology, Vol. 22
Edited by J. Lewins and M. Becker, Plenum Press, New York, 1991

In this work we shall summarize the knowledge recently gained about how the intensity due to multiple scattering perturbs the first-order terms of the three processes of main interest in X-ray spectrometry between 1 keV and 100 keV: the photoelectric, the Rayleigh and the Compton effects. We shall show that the contribution of a few orders of scattering, calculated in the frame of transport theory, allows the construction of a theoretical X-ray spectrum that matches well experimental data from targets of homogeneous composition and infinite thickness. The calculations are performed analytically using an exact iterative solution, universally valid with all types of interactions, which practically introduces the formal use of transport theory in the field. The main symbols are listed at the end of the paper. The results obtained allow us to quantify the importance of multiple scattering of the Rayleigh and Compton effects that overlap the Compton line, to compute scattering contributions to the characteristic XRF lines, and to evaluate higher orders of purely photoelectric interactions, which are useful in IXSS and EDXRF respectively. But what is more important, they confirm that the techniques of transport thus can be successfully used to obtain refined solutions in problems of X-ray spectrometry, opening a new line of applications in this field.

2. RELEVANT ASPECTS OF PHOTON INTERACTIONS WITH MATTER

Photons can interact in different ways depending on their energy *(1-3)*. The photons in the X-ray regime interact with the electron shells which surround the nucleus. The nucleus itself does not contribute to the scattering or absorption of photons.

The interaction of a photon of energy $h\nu$ with an isolated atom A has the effect of changing the atom's state from $|i\rangle$ to $|f\rangle$, which can be expressed as

$$A_i + h\nu_i \rightarrow A_f + h\nu_f \quad . \tag{1}$$

Eqn (1) denote the type of photon-atom interactions of interest in this work, having one initial photon and only one resulting photon. A_f denotes the atom plus all the non-photonic particles produced in the reaction.

There are three photon-atom processes whose influence prevail in the X-ray regime *(4-6)*: the *photoelectric effect* in which the photons cause the ejection of an electron leaving a hole in the atom which, when the vacancy is filled by another

electron, emits a fluorescence photon having the energy difference between the electron and the hole levels; the *unmodified or Rayleigh scattering* in which the photon changes momentum but not energy; and the *modified or Compton scattering* in which both momentum and energy are transferred to the electrons comprising the atom.

What we call an interaction may not be strictly a single process. Any sequence of physical processes in rapid succession, originated by a photon and producing another(other) photon(s), can be statistically considered as an unique interaction, as occurring for example with the photoelectric effect.

The resulting (or secondary) photon from the interactions may collide in turn with another atom, starting a multiple chain of events that we want to study. However, not only photons are produced in the photon-atom interactions. The photoelectric effect and the modified scattering produce electrons which, obeying other kind of interactions, can produce new photons. Since these contributions render the transport problem far more complicated because of the coupling between photons and electrons, we shall neglect in this work bremsstrahlung (braking radiation) of the Compton and photoelectric electrons *(7)*, and also other photon sources such as anomalous scattering *(8)* and pair production-annihilation.

The single-process kernels play a very important role in transport theory. They represent the probability density - by unit wavelength, by unit solid angle, and by unit path - that the process may change the phase-space variables from $(\vec{\omega}',\lambda')$ to $(\vec{\omega},\lambda)$. Therefore a kernel is directly related to the double-differential scattering coefficient of the interaction. Thus, the scattering coefficient for the process T can be obtained from

$$\sigma_T(\lambda',\vec{\omega}') = \int_0^\infty d\lambda \int_{4\pi} d\omega \; k_T(\vec{\omega},\lambda,\vec{\omega}',\lambda') \quad , \tag{2}$$

allowing the comparison with experimental or theoretical data. Since the processes of interest are statistically independent, and since they constitute the main part of the total attenuation coefficient *(9-12)* as can be appreciated even in the most recent compilations *(13-14)*, we can define the total attenuation coefficient as

$$\mu = \sigma_C + \sigma_R + \tau \quad , \tag{3}$$

where σ_C and σ_R are the Compton (incoherent) and Rayleigh (coherent) integral attenuation coefficients and τ is the photoelectric attenuation coefficient.

If we consider attenuation of photons, then at low energies atomic photoelectric effects predominate, while at intermediate energies Compton scattering dominates. If, however, we are concerned with scattering of photons, then Rayleigh scattering dominates at low energies or forward angles, while Compton scattering dominates at higher energies or larger angles.

In what follows we shall write the atomic interaction kernels for the three dominating processes that participate in X-ray photon transport. Since our aim is to explain the contribution of multiple scattering terms, we shall use coherent and incoherent scattering factors to describe atomic modification (electron binding and electronic charge distribution) of the single-electron scattering cross-sections. The form factor approximation associates a smooth behaviour to the scattering cross-sections that cannot explain scattering resonances *(15)*, but it gives a quite detailed view of the atomic effects on the scattering of photons. On the other hand, we shall not consider the motion of the electrons in the atom which could complicate the transport equation. However, at least for the incoherent case, the scattering factor can be obtained with an integration of momentum profiles of single orbitals *(16)* giving a simple connection between the Compton profiles and the corresponding scattering factor. Polarization effects will be not considered because they require a complicated formulation of the transport problem that is out of the scope of this work.

2.1. Photoelectric effect

The photoelectric effect is an indirect photon-photon process. The absorption of a photon by photoelectric effect creates a hole in the atom that ejects an electron with some kinetic energy. The vacancy may be spontaneously filled by means of an electron transition from a higher energy level, with emission of a characteristic photon. Statistically, the two combined processes may be considered as a single interaction. The theory of the photoionization process has received great attention *(17,18)*, the photoelectric cross-section has been largely investigated with experiments and theoretical calculations *(19)*, and collected data are available elsewhere *(13,20)*.

The kernel for a single XRF characteristic line *(21,22)* of wavelength λ_i emitted by a pure element target s as a consequence of photoelectric absorption of photons with wavelength λ' is given by *(23)*

$$k_{P_{\lambda_i}}(\vec{\omega},\lambda,\vec{\omega}',\lambda') = \frac{1}{4\pi} Q_{\lambda_i}(\lambda')\ \delta(\lambda-\lambda_i)\ [1-\mathcal{U}(\lambda'-\lambda_{e_i})]\ , \qquad (4)$$

The isotropy of the photoelectric effect is reflected by the kernel independence on $\vec{\omega}$ and by the 4π normalization factor. The line is assumed monochromatic, neglecting its natural width *(24)* that is significantly lower than the instrumental one *(25)*. The XRF emission probability density $Q_{\lambda_i}(\lambda')$ for the line λ_i (in $[cm^{-1}]$) is given by the probability relation

$$Q_{\lambda_i}(\lambda') = \tau_s(\lambda')\ (1-1/J_{\lambda_i})\ \omega_{\lambda_i}\ \Gamma_{\lambda_i}\ , \qquad (5)$$

where $\tau_s(\lambda')$ is the photoelectric attenuation coefficient (in $[cm^{-1}]$) of the emitter element s *(9-11,13,14,20)*, $J_{\lambda i}$ is the absorption-edge jump *(9-11,13,14,20)*, $\omega_{\lambda i}$ the fluorescence yield *(26-31)*, and $\Gamma_{\lambda i}$ the line emission probability of the line at λ_i into its own spectral series *(32-36)*. The line is emitted only when λ' is lower than the threshold of the absorption edge wavelength λ_{ei} of the series to which the line belongs *(9-11,13,14,20,22)*, as the Heaviside function $\mathcal{U}$ in Eqn (4) expresses.

The complete emission spectrum of the element s is obtained adding all the single line terms:

$$k_P(\vec{\omega},\lambda,\vec{\omega}',\lambda') = \frac{1}{4\pi} \sum_i Q_{\lambda_i}(\lambda')\ \delta(\lambda-\lambda_i)\ [1-\mathcal{U}(\lambda'-\lambda_{e_i})]\ . \qquad (6)$$

2.2. Coherent (Rayleigh) scattering

The coherent scattering is a process where the photons change direction but not energy *(37)*. This scattering takes place with the more bound electrons of the atom which behave rigidly during the interaction. The Rayleigh atomic kernel for unpolarized photons, with phase-space coordinates $(\vec{\omega}',\lambda')$ scattered by a pure element target with atomic number Z into the coordinates $(\vec{\omega},\lambda)$, is *(38)*

$$k_R(\vec{\omega},\lambda,\vec{\omega}',\lambda') = \sigma\,\delta(\lambda-\lambda')\left[1+(\vec{\omega}\cdot\vec{\omega}')^2\right]\frac{F^2(\lambda',\vec{\omega}\cdot\vec{\omega}',Z)}{Z}, \quad (7)$$

where $\sigma = \rho N Z r_0^2/(2A)$ is a macroscopic attenuation coefficient (in $[cm^{-1}]$), r_0 being the classical radius of the electron, ρ the density, N Avogadro's number and A the atomic weight. The delta function stresses the monocromaticity of the scattering. The angular dependence of the kernel (7) is due to the last two factors: the Thompson angular factor, and the atomic form factor comprising the constructive interference from the whole charge distribution. The coherent form factor $F(\lambda',\vec{\omega}\cdot\vec{\omega}',Z)$ can explain atomic contributions that are significantly greater than Z times the contribution from one single electron. Special limits are $F(\lambda',1,Z) = F(\infty,\vec{\omega}\cdot\vec{\omega}',Z) = Z$ and $F(0,\vec{\omega}\cdot\vec{\omega}',Z) = 0$. Experimental data tables of form factors and references to theoretical computations for many electron atoms may be found in the classical paper of Hubbell et al. *(39)* and in more recent works *(40,41,37)*. A closed expression *(42)* giving approximate values for F is available. More precise values are achieved with semi-empirical formulae and fitting coefficients of theoretical calculations *(43)*.

2.3. Incoherent (Compton) scattering

In incoherent scattering, energy as well as direction is changed *(44,45)*. This process takes place with the outer electrons of the atom. The Compton atomic kernel for incident photons, with phase-space coordinates $(\vec{\omega}',\lambda')$ scattered by a pure specie target of atomic number Z into the coordinates $(\vec{\omega},\lambda)$, is *(38)*

$$k_C(\vec{\omega},\lambda,\vec{\omega}',\lambda') = \sigma\,K_{KN}(\lambda,\lambda')\,S(\lambda',\vec{\omega}\cdot\vec{\omega}',Z)\,\frac{1}{\lambda_C}\,\delta\left(1-\vec{\omega}\cdot\vec{\omega}'+\frac{\lambda'-\lambda}{\lambda_C}\right), \quad (8)$$

where

$$K_{KN}(\lambda,\lambda') = \left(\frac{\lambda'}{\lambda}\right)^2\left\{\frac{\lambda}{\lambda'}+\frac{\lambda'}{\lambda}+\frac{\lambda-\lambda'}{\lambda_C}\left(\frac{\lambda-\lambda'}{\lambda_C}-2\right)\right\}, \quad (9)$$

and $\lambda_C = 0.0242631$ Å is the Compton wavelength. The $\sigma\,K_{KN}(\lambda,\lambda')$ factor denotes the well known Klein-Nishina differential coefficient *(46)*. The direction-wavelength delta fixes the integration path in the phase-space along the line $1-\vec{\omega}\cdot\vec{\omega}'+(\lambda'-\lambda)/\lambda_C = 0$ (this condition does not account for the shift for bound electrons *(45)*). $S(\lambda',\vec{\omega}\cdot\vec{\omega}',Z)$ is an incoherent scattering form factor taking into account the electron binding. Some special limits are $S(\lambda,1,Z) = S(\infty,\vec{\omega}\cdot\vec{\omega}',Z) = 0$ and $S(0,\vec{\omega}\cdot\vec{\omega}',Z) = 1$. Data tables and references to theoretical computations are found in the paper of Hubbell et al. *(39)* (note that their 'scattering function' means S Z here). A closed approximate formula for S was obtained *(42)* with the Thomas-Fermi model. Precise values of the S factor can be computed with semi-empirical formulas and fitting coefficients to theoretical calculations *(47)*.

The pre-collision motion of the electrons has been ignored in the kernel (8), limiting the Compton peak to a monochromatic line. The more rigorous theoretical treatment associated with the Compton profile is not sufficiently tractable for extensive calculation and will not be considered here. However, the multiple scattering effects will be better appreciated in a context of generality, independent of the state of excitation of the atom and the chemical bond to other atoms.

2.4. The total kernel

According to our previous assumptions about the composition of the total attenuation coefficient we can write an expression, analogous to (3), for the total interaction kernel of photons in the X-ray regime

$$k(\vec{\omega},\lambda,\vec{\omega}',\lambda') = k_R(\vec{\omega},\lambda,\vec{\omega}',\lambda') + k_C(\vec{\omega},\lambda,\vec{\omega}',\lambda') + \sum_i k_{P_{\lambda_i}}(\vec{\omega},\lambda,\vec{\omega}',\lambda'), \quad (10)$$

which, integrated as in (2), allows us to recover the radiative part of Eqn (3).

Up to now, we have considered the above kernels in the pure element with atomic number Z. We will now analyze how they transform for materials composed by several species of atoms.

We denote by W_j the *weight fraction* of the element j which satisfies the relationship

$$\sum_j W_j = 1, \quad (11)$$

The mass attenuation coefficient (in [cm^2/g]) for a composite material obeys the well known relation *(1,4)*

$$\frac{\mu}{\rho} = \sum_j W_j \left(\frac{\mu}{\rho}\right)_j , \qquad (12)$$

where μ is the total atenuation coefficient given by Eqn (3) and $(\mu/\rho)_j$ is the total mass attenuation coefficient for the single element j. The coefficients of the partial interactions follow a similar relationship.

The total kernel for a composite material is easily obtained from the kernels for the single sample components replacing *all the attenuation coefficients by mass attenuation coefficients in Eqns (6), (7) and (8)*

$$k(\vec{\omega},\lambda,\vec{\omega}',\lambda') = \sum_j W_j \left\{ k_R(\vec{\omega},\lambda,\vec{\omega}',\lambda') \Big|_j + k_C(\vec{\omega},\lambda,\vec{\omega}',\lambda') \Big|_j + \sum_i k_{P_{\lambda_i}}(\vec{\omega},\lambda,\vec{\omega}',\lambda') \Big|_j \right\}, \qquad (13)$$

where $k_a(\vec{\omega},\lambda,\vec{\omega}',\lambda') \Big|_j$ represents the 'mass' kernel for the interaction a with the specie of atoms Z_j.

3. TIME-INDEPENDENT PHOTON TRANSPORT EQUATION

The flow of X-rays is completely determined as the solution of a transport equation describing the balance between the number of photons of given energy and direction entering and leaving an infinitesimal volume element. This balance may be formulated for conditions where the X-ray source is constant in time (steady-state problem) and, therefore, also the photon flow in the medium.

3.1. The photon transport equation for an infinite medium

Let us consider a point $\vec{r}$ and an infinitesimal right cylinder with a base area dA centred at $\vec{r}$ and with a height $d\ell$, whose lateral surface is parallel to a direction $\vec{\omega}$. We define the flux $f(\vec{r},\vec{\omega},\lambda)\, d\lambda\, d\omega$ as the number of photons with wavelengths between λ and $\lambda + d\lambda$, and with directions between $\vec{\omega}$ and $\vec{\omega} + d\vec{\omega}$, which cross a unit area of the base of the infinitesimal cylinder per unit time.

We shall use the wavelength λ in place of the energy E because it is more convenient to describe the above interactions, although the use of E should be entirely equivalent *(48)*. This choice will also allow us to maintain close compatibility with previous results. We should not forget that spectroscopic techniques evolved much earlier in the wavelength domain that in the energy domain. Besides, it is always possible to convert the results from wavelength to energy domain with an appropriate transformation.

The net number of photons with specified direction and energy leaving the infinitesimal cylinder per unit time is represented by the quantity

$$f(\vec{r} + \vec{\omega}\, d\ell,\vec{\omega},\lambda)\, dA - f(\vec{r},\vec{\omega},\lambda)\, dA , \qquad (14)$$

which can be expressed in differential form

$$\vec{\omega}\cdot\nabla f(\vec{r},\vec{\omega},\lambda)\, dA\, d\ell . \qquad (15)$$

Three factors contribute to this net outflow:

i) The *narrow-beam attenuation in the whole volume of the cylinder*, which amounts to $-\mu(\lambda)\, d\ell\, f(\vec{r},\vec{\omega},\lambda)\, dA$. Narrow-beam attenuation is ruled by the known one-dimensional Beer-Lambert attenuation law. $\mu(\lambda)$, the specimen's total mass attenuation coefficient, is strongly wavelength(energy)-dependent, but it is independent of geometry, because measurements of narrow-beam attenuation coefficients are performed with the classic experiment of intensity attenuation by thin absorber foils.

ii) The *scattering* of photons with direction $\vec{\omega}'$ and wavelength λ' into $\vec{\omega}$ and λ. If the scattering happens anywhere within the cylinder volume $dA\, d\ell$, it contributes a positive outflow from the cylinder. This term depends on the flow $f(\vec{r},\vec{\omega},\lambda)$ times the probability density function $k(\vec{\omega},\lambda,\vec{\omega}',\lambda')$ of photon scattering into $\vec{\omega}$ and λ from $\vec{\omega}'$ and λ' (per unit path through the medium and per unit $d\omega$ and $d\lambda$). The product must be integrated over all incident directions $\vec{\omega}'$ and wavelengths λ' to give the whole scattering contribution.

The word 'scattering' denotes some generic process capable of transmuting a photon of some energy and direction into another photon with different (or equal) energy and direction (see Eqn (1)), and does not strictly mean a

scattering process. In this sense, the radiative photoeffect responsible of the XRF emission may be considered a scattering process.

iii) The *source*, if any, introduces photons with a given energy and direction within the cylinder.
If the photons are produced with a source density $\mathcal{S}(\vec{r},\vec{\omega},\lambda)$, per unit volume, per unit time, per steradian and per unit λ, the corresponding excess flow out of the cylinder will be $dA\, d\ell\, \mathcal{S}(\vec{r},\vec{\omega},\lambda)$, per unit time, per steradian and per unit λ.

Equating the difference (15) to the sum of the above three factors and factoring out the arbitrary cylindrical volume $dA\, d\ell$, we obtain the transport equation for photons

$$\vec{\omega}\cdot\nabla f(\vec{r},\vec{\omega},\lambda) = -\mu(\lambda) f(\vec{r},\vec{\omega},\lambda) + \int_0^\infty d\lambda' \int_{4\pi} d\omega' k(\vec{\omega},\lambda,\vec{\omega}',\lambda') f(\vec{r},\vec{\omega}',\lambda') + \mathcal{S}(\vec{r},\vec{\omega},\lambda) \quad . \tag{16}$$

Although Equation (16) is quite general, it corresponds to an infinite geometry. In general, the functions μ, k and S will depend on the medium composition, on the interactions, on the geometry of interest, and on the excitation source. The required degree of approximation also plays a role in the solution since the mathematical difficulty in obtaining an analytical solution to the integro-differential Eqn (16) is very high. When the geometry and the shapes of μ, k and S, do not satisfy the conditions which, rarely, make an analytical solution possible, it is customary to solve the equation with approximate or numerical methods.

3.2. The transport equation for the model

We shall adapt the Eqn (16) to represent the diffusion of a monochromatic and collimated X-ray beam in a thick homogeneous target. Following Fano, Spencer and Berger *(49)*, the transport equation for an incident beam of parallel rays (with flight direction $\vec{\omega}_0$) hitting the infinite sample surface, reduces to a one-dimensional spatial equation. The monochromatic beam of wavelength λ_0 is represented by a Dirac δ-function $\delta(\lambda-\lambda_0)$ and the collimation in the direction $\vec{\omega}_0$ by $\delta(\vec{\omega}-\vec{\omega}_0)$. Since a plane through the point $\vec{r}_0$ and perpendicular to $\vec{u}$ has the equation $\vec{u}\cdot\vec{r} = \vec{u}\cdot\vec{r}_0$, a source of I_0 uniformly

distributed photons $cm^{-2}\, s^{-1}$ on this plane is represented by the function $I_0\, \delta(\vec{u}\cdot\vec{r}-\vec{u}\cdot\vec{r}_0)$. Then, the complete source term can be written as

$$\mathcal{S}(\vec{r},\vec{\omega},\lambda) = I_0\, \delta(\vec{u}\cdot\vec{r}-\vec{u}\cdot\vec{r}_0)\, \delta(\vec{\omega}-\vec{\omega}_0)\, \delta(\lambda-\lambda_0) \quad . \tag{17}$$

The flux calculation is easier when the medium is infinite and homogeneous, that is, when the coefficients μ and k take the same values through all the space. Under this assumption, if the source function depends spatially on the component of $\vec{r}$ along $\vec{\Omega}$ ($\vec{\Omega}$ being some arbitrary direction), the flux distribution has the same plane of symmetry, i.e. it depends on the single space coordinate $\vec{r}\cdot\vec{\Omega}$. Therefore, we can eliminate two spatial variables in the transport Eqn (16) by choosing the point $\vec{r}_0$ as the origin of coordinates and the direction $\vec{u}$ as the z axis. In this way the spatial flux distribution will depend only on z and $\vec{\omega}\cdot\nabla f$ will reduce to $\omega_z(\partial f/\partial z)$.

The transport equation can also be adapted, preserving the above conditions, to describe the diffusion in a semi-infinite medium. To this end, we assume the source is just placed along the plane interface between two infinite semi-spaces: an infinite empty region over the infinite target. A sketch of the geometrical arrangement is shown in figure 1.

So far, as we are concerned with photons interacting in the target (positive z), we can assume that the photons escaping towards the upper side may suffer absorption but cannot be backscattered into the target. This model *(50)* represents fairly well the behaviour of radiation in two media of different density (the density in the sample being much greater than the density in the surrounding empty space or air).

Such a model can be well represented replacing the kernel $k(\vec{\omega},\lambda,\vec{\omega}',\lambda')$ by a new one including explicitly this spatial dependence. The new kernel should take the value zero for negative z (because photons in the upper semi-space have zero probability of being scattered) while it should match the old kernel in the lower semi-space. Consequently, the empty semi-space is figured in the equation through its non restitution property, rather than by a change in the density or in the absorption coefficient. This choice preserves the mathematical shape of Eqn (16) while ensuring a uniform $\mu(\lambda)$.

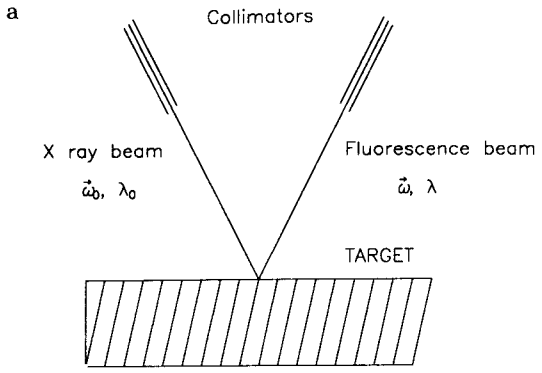

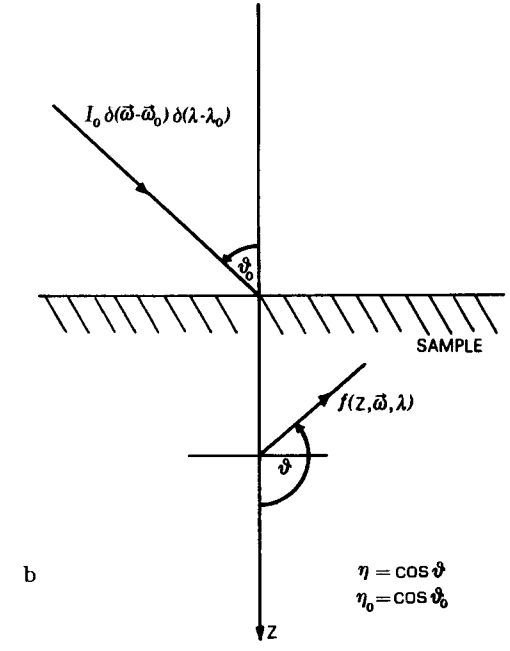

Figure 1.(a) Irradiation scheme of an homogeneous specimen of infinite thickness excitted with a collimated monochromatic X-ray source.

Figure 1.(b) The magnitudes represented in the photon transport equation (18).

The one-dimensional Boltzmann equation for the model is

$$\eta\frac{\partial f(z,\vec{\omega},\lambda)}{\partial z} =$$

$$-\mu(\lambda)\, f(z,\vec{\omega},\lambda) + \int_0^{\infty} d\lambda' \int_{4\pi} d\omega'\; k(\vec{\omega},\lambda,\vec{\omega}',\lambda')\; \mathcal{U}(z)\; f(z,\vec{\omega}',\lambda')$$

$$+ I_0\, \delta(z)\, \delta(\vec{\omega}-\vec{\omega}_0)\, \delta(\lambda-\lambda_0)\ , \qquad (18)$$

where η denotes the director cosine ω_z, $d\omega' = d\eta' d\varphi'$ the differential of solid angle in the direction of the unitary vector $\vec{\omega}'$ and $\mathcal{U}(z)$ the unitary step Heaviside function.

It should be noted that, although the transport Eqn (18) is one-dimensional, the flux maintains all the angular information through its dependence on $\vec{\omega}$.

4. SOLUTION IN A HALF SPACE: MULTIPLE SCATTERING EFFECTS

A well known method *(49,51-55)* to solve the transport equation consists in determining separately the flux of the primaries and the flux of particles scattered once, twice, and so on. Although this approach leads naturally to a multiple scattering solution, it has been rarely used to obtain analytical solutions. This is mainly because the Boltzmann equation has been intensively applied in neutron transport, where this kind of solution is of scarse interest unless the multiple scattering terms have a sufficiently high convergence speed, and where, in every case, it must compete with more efficient approximate techniques. Furthermore, the geometries of interest in neutron transport normally require the use of numerical, not analytical methods. On the other hand, the single terms obtained with this kind of solution in neutron transport cannot be easily associated with distinctive characteristics of the neutron interactions. However, the power of this approach is largely acknowledged since it constitutes the foundation of the Monte Carlo method of simulation *(49,55,56)*, which has become the most intensively used method with every kind of particle transport problem.

The search for an analytical solution for multiple scattering in photon transport has a different meaning than for neutrons, since we are particularly interested in investigating how the higher scattering terms modify the first order of

emission for each type of process. What renders this study more interesting is that X-ray spectrometry offers the rare occasion of individualizing some contributions of multiple scattering.

4.1. The multiple scattering solution

If we set

$$f = f^{(0)} + f^{(1)} + f^{(2)} + \ldots , \tag{19}$$

and substitute (19) in (18) we obtain a system of equations. The equation for the primary flux $f^{(0)}$ is obtained deleting the integral in Eqn (18). Using the Kronecker delta δ_{n0}, we can write the generic equation for $f^{(n)}$

$$\eta \frac{\partial f^{(n)}(z,\vec{\omega},\lambda)}{\partial z} = -\mu(\lambda)\, f^{(n)}(z,\vec{\omega},\lambda)$$

$$+ \int_0^\infty d\lambda' \int_{4\pi} d\omega'\; k(\vec{\omega},\lambda,\vec{\omega}',\lambda')\; \mathcal{U}(z)\; f^{(n-1)}(z,\vec{\omega}',\lambda')\; [1-\delta_{n0}]$$

$$+ I_0\, \delta(z)\, \delta(\vec{\omega}-\vec{\omega}_0)\, \delta(\lambda-\lambda_0)\, \delta_{n0}, \qquad n = 0, 1, 2, \ldots \tag{20}$$

The sum of the equations for n = 0, 1, ... is identical with Eqn (18).

To solve the Eqns (20) we shall split the flux $f^{(n)}(z,\vec{\omega},\lambda)$ into its even, $f_+^{(n)}(z,\vec{\omega},\lambda)$, and odd, $f_-^{(n)}(z,\vec{\omega},\lambda)$, spatial parts, and we shall use $\mathcal{U}(z) = (1 + \text{sgn } z)/2$ to obtain

$$\eta \frac{\partial}{\partial z} f_-^{(n)} = -\mu(\lambda)\, f_+^{(n)} + \left[\frac{1}{2}\hat{I} f_+^{(n-1)} + \frac{1}{2}\hat{I}\ \text{sgn } z\ f_-^{(n-1)}\right][1-\delta_{n0}]$$

$$+ I_0\, \delta(z)\, \delta(\vec{\omega}-\vec{\omega}_0)\, \delta(\lambda-\lambda_0)\, \delta_{n0} , \tag{21a}$$

$$\eta \frac{\partial}{\partial z} f_+^{(n)} = -\mu(\lambda)\, f_-^{(n)} + \left[\frac{1}{2}\hat{I} f_-^{(n-1)} + \frac{1}{2}\hat{I}\ \text{sgn } z\ f_+^{(n-1)}\right][1-\delta_{n0}] , \tag{21b}$$

where $\hat{I}$ is the integral operator of Eqn (18), which neither commutes with $f_+^{(n)}$ nor with $f_-^{(n)}$, but with any function of z only (i.e. with sgn z).

Equations (21) can be Fourier-transformed, giving

$$iq\eta\, \tilde{f}_-^{(n)} = -\mu(\lambda)\, \tilde{f}_+^{(n)} + \left[\frac{1}{2}\hat{I}\, \tilde{f}_+^{(n-1)} + \frac{1}{2}\hat{I}\, \mathcal{F}[\text{sgn } z] \otimes \tilde{f}_-^{(n-1)}\right][1-\delta_{n0}]$$

$$+ I_0\, \delta(\vec{\omega}-\vec{\omega}_0)\, \delta(\lambda-\lambda_0)\, \delta_{n0} , \tag{22a}$$

and

$$iq\eta\, \tilde{f}_+^{(n)} = -\mu(\lambda)\, \tilde{f}_-^{(n)} + \left[\frac{1}{2}\hat{I}\, \tilde{f}_-^{(n-1)} + \frac{1}{2}\hat{I}\, \mathcal{F}[\text{sgn } z] \otimes \tilde{f}_+^{(n-1)}\right][1-\delta_{n0}], \tag{22b}$$

where the symbol $\otimes$ denotes a convolution product and $\tilde{f}_\pm^{(n)}(q,\vec{\omega},\lambda)$ is the Fourier transform of the flux $f_\pm^{(n)}(z,\vec{\omega},\lambda)$. If we introduce the integral operator $\hat{K}$, the indicated convolution can be written as

$$\mathcal{F}[\text{sgn } z] \otimes \tilde{f}_\pm^{(n-1)}(q,\vec{\omega},\lambda) = \frac{1}{\pi}\int_{-\infty}^{\infty} d\tau \frac{1}{i(q-\tau)}\, \tilde{f}_\pm^{(n-1)}(\tau,\vec{\omega},\lambda)$$

$$= -i\, \hat{K}\, \tilde{f}_\pm^{(n-1)}(\tau,\vec{\omega},\lambda) , \tag{23}$$

and the set of equations (22) becomes

$$iq\eta\, \tilde{f}_-^{(n)} = -\mu(\lambda)\, \tilde{f}_+^{(n)} + \left[\frac{1}{2}\hat{I}\, \tilde{f}_+^{(n-1)} - \frac{i}{2}\hat{I}\,\hat{K}\, \tilde{f}_-^{(n-1)}\right][1-\delta_{n0}]$$

$$+ I_0\, \delta(\vec{\omega}-\vec{\omega}_0)\, \delta(\lambda-\lambda_0)\, \delta_{n0} , \tag{24a}$$

$$iq\eta\, \tilde{f}_+^{(n)} = -\mu(\lambda)\, \tilde{f}_-^{(n)} + \left[\frac{1}{2}\hat{I}\, \tilde{f}_-^{(n-1)} - \frac{i}{2}\hat{I}\,\hat{K}\, \tilde{f}_+^{(n-1)}\right][1-\delta_{n0}]. \tag{24b}$$

For n = 0, Eqns (24) give

$$iq\eta\, \tilde{f}_-^{(0)} = -\mu(\lambda)\, \tilde{f}_+^{(0)} + I_0\, \delta(\vec{\omega}-\vec{\omega}_0)\, \delta(\lambda-\lambda_0) , \tag{25a}$$

$$iq\eta\, \tilde{f}_+^{(0)} = -\mu(\lambda)\, \tilde{f}_-^{(0)} , \tag{25b}$$

from which

$$\tilde{f}_+^{(0)} = \frac{\mu}{\mu^2 + q^2\eta^2}\, I_0\, \delta(\vec{\omega}-\vec{\omega}_0)\, \delta(\lambda-\lambda_0) , \tag{26a}$$

$$\tilde{f}_{-}^{(0)} = \frac{-iq\eta}{\mu^2 + q^2\eta^2} I_o \, \delta(\vec{\omega}-\vec{\omega}_o) \, \delta(\lambda-\lambda_o) \quad . \tag{26b}$$

The solution in the physical space is obtained using the Fourier inversion formula for real functions

$$f^{(0)}(z,\vec{\omega},\lambda) =$$

$$\frac{I_o}{2|\eta|} \, \delta(\vec{\omega}-\vec{\omega}_o) \, \delta(\lambda-\lambda_o) \, \exp\left[-\frac{\mu|z|}{|\eta|}\right] \, (1 + \text{sgn}\ \eta \ \text{sgn}\ z) \quad , \tag{27}$$

For n > 0, Eqns (24) have the matrix expression

$$\begin{pmatrix} iq\eta & \mu \\ \mu & iq\eta \end{pmatrix} \begin{pmatrix} \tilde{f}_{-}^{(n)} \\ \tilde{f}_{+}^{(n)} \end{pmatrix} = \frac{\hat{I}}{2} \begin{pmatrix} -i\hat{K} & 1 \\ 1 & -i\hat{K} \end{pmatrix} \begin{pmatrix} \tilde{f}_{-}^{(n-1)} \\ \tilde{f}_{+}^{(n-1)} \end{pmatrix} \quad . \tag{28}$$

Calling the square matrices of the previous equation $\mathbb{A}$ and $\mathbb{K}$ respectively, and $\mathbb{P}$ the projection operator which maps $\tilde{f}^{(n)}$ into the column vector $(\tilde{f}_{-}^{(n)}, \tilde{f}_{+}^{(n)})^T$, the above equation can be reduced to

$$\mathbb{A}\,\mathbb{P}\,\tilde{f}^{(n)} = \frac{\hat{I}}{2}\,\mathbb{K}\,\mathbb{P}\,\tilde{f}^{(n-1)} \quad . \tag{29}$$

Using the last equation recursively, we can write an expression for $\tilde{f}$ in terms of $\tilde{f}^{(0)}$:

$$\mathbb{P}\,\tilde{f} = \sum_{n=1}^{\infty} 2^{1-n} \, [\mathbb{A}^{-1}\mathbb{K}\,\hat{I}]^{n-1} \, \mathbb{P}\,\tilde{f}^{(0)} \quad . \tag{30}$$

In the physical space we have

$$\begin{aligned} \mathbb{P}f^{(n)} &= \frac{\hat{I}}{2}\,\mathcal{R}e\,\mathcal{F}^{-1}\left\{\mathbb{A}^{-1}\right\} \otimes \mathcal{F}^{-1}\left\{\mathbb{K}\mathbb{P}\tilde{f}^{(n-1)}\right\} \\ &= \frac{\hat{I}}{2}\,\mathcal{R}e\,\mathcal{F}^{-1}\left\{\mathbb{A}^{-1}\right\} \otimes \left\{(1+\text{sgn}z)\mathbb{P}\tilde{f}^{(n-1)}\right\} \quad , \end{aligned} \tag{31}$$

where the convolution property of the Fourier transforms has been used. Due to the noncommutability of the RHS matrix operator with the projection $\mathbb{P}$ operator, it becomes clear that both the even part of the nth-order solution and the odd part depend on both the even *and* the odd parts of the (n-1)th-order solution. This means that solution parity can never be preserved at any order, because successive orders will destroy such a property.

Solving for the inverse transform of $\mathbb{A}^{-1}$ and expressing the convolution product as an integral, we can finally write the nth-order flux $f^{(n)}$ as

$$f^{(n)}(z,\vec{\omega},\lambda) = \frac{1}{2|\eta|} \int_0^{\infty} d\tau \int_0^{\infty} d\lambda' \int_{4\pi} d\omega' \ k(\vec{\omega},\lambda,\vec{\omega}',\lambda') \ \exp\left(-\frac{|z-\tau|\mu}{|\eta|}\right)$$

$$(1 + \text{sgn}\ \eta \ \text{sgn}\ (z-\tau)) \ f^{(n-1)}(\tau,\vec{\omega}',\lambda') \quad . \tag{32}$$

It is worth noting that *no assumption has been made on the kernel shape* other than having made explicit its dependence on z through the Heaviside step function. This fact renders the above solution very general since it can be calculated with *any* kind of interaction kernel.

In practice, it is easier to employ an expression equivalent to (32) where the integral over z has been divided into two parts, according to the sign of $(z-\tau)$. In this way, the solution corresponding to *positive* z is

$$f^{(n)}(z,\vec{\omega},\lambda) = \frac{1}{|\eta|}$$

$$\left\{\frac{(1+\text{sgn}\ \eta)}{2} \exp\left(-\frac{z\mu}{|\eta|}\right)\right.$$

$$\int_0^{z} d\tau \ \exp\left(\frac{\tau\mu}{|\eta|}\right) \int_0^{\infty} d\lambda' \int_{4\pi} d\omega' \ k(\vec{\omega},\lambda,\vec{\omega}',\lambda') \ f^{(n-1)}(\tau,\vec{\omega}',\lambda')$$

$$+ \frac{(1-\text{sgn}\ \eta)}{2}$$

$$\left.\int_0^{\infty} d\tau \ \exp\left(-\frac{\tau\mu}{|\eta|}\right) \int_0^{\infty} d\lambda' \int_{4\pi} d\omega' \ k(\vec{\omega},\lambda,\vec{\omega}',\lambda') \ f^{(n-1)}(\tau+z,\vec{\omega}',\lambda')\right\} \quad , \tag{33}$$

and the solution *for negative z* is

$$f^{(n)}(z,\vec{\omega},\lambda) = \frac{1}{|\eta|}\,\frac{(1-\mathrm{sgn}\ \eta)}{2}\,\exp\left(-\frac{|z|\mu}{|\eta|}\right)$$

$$\int_0^\infty d\tau\ \exp\left(-\frac{\tau\mu}{|\eta|}\right)\int_0^\infty d\lambda'\int_{4\pi} d\omega'\ k(\vec{\omega},\lambda,\vec{\omega}',\lambda')\ f^{(n-1)}(\tau,\vec{\omega}',\lambda')\ . \qquad (34)$$

Because of the recursive character of Eqns (33) and (34), to compute every new order solution we need to know the previous order solution.

For z = 0 (negative η) we obtain the solution for reflected radiation (the so-called albedo solution). Both the positive- and the negative-z solutions coincide in that point. Therefore, we could use either solution (33) or (34) to calculate the albedo partial solution. Solution (33) certainly has a more interesting physical meaning, because it allows one to compute the angular flux *into the target*. Since (34) also requires the (n-1)th solution for positive z, a knowledge of the positive-z solution is always essential to calculate the next order.

4.2. Relation between flux and intensity

To make the comparison between a transport equation solution and a customary X-ray spectrometric intensity feasible, we must state a relationship between the flux and the intensity.

The partial intensity, defined as the number of photons passing through a surface element per unit time, can be obtained as the partial current of the flux through the surface at z = 0 (albedo flux) in the given direction *(53)*. Therefore it is given by the positive-defined quantity

$$I^{(n)}(\vec{\omega},\lambda) = |\eta|\ f^{(n)}(0,\vec{\omega},\lambda)\ . \qquad (35)$$

The partial intensity $I^{(n)}$ gives the number of photons (of n-th order) per unit time, unit surface, unit solid angle and unit wavelength, having angular direction $\vec{\omega}$ and wavelength λ; it therefore offers full information about the angular and spectral properties of the emitted radiation. In a similar way we define the wavelength-integrated intensity

$$\mathfrak{I}^{(n)}(\vec{\omega}) = \int_0^\infty d\lambda\ I^{(n)}(\vec{\omega},\lambda)\ , \qquad (36)$$

that totals the spectral information and gives the magnitude of the whole partial intensity emitted in the direction $\vec{\omega}$.

4.3. The intensity for double scattering

An explicit relationship for the second-order intensity can be derived from Eqns (27), (33) and (35), for the total kernel (10). Splitting the kernel into single processes, it is possible to obtain *(38)* a general expression for the second-order intensity (corresponding to the chain of interactions *a* and *b*, occurring in this order)

$$I^{(2)}_{(a,b)}(\vec{\omega},\lambda) = \frac{(1-\mathrm{sgn}\ \eta)}{2}\,\frac{(1+\mathrm{sgn}\ \eta_0)}{2}\,\frac{I_0}{|\eta_0|}\,\frac{1}{\dfrac{\mu}{|\eta|}+\dfrac{\mu_0}{|\eta_0|}}$$

$$\int_0^\infty d\lambda'\int_{4\pi} d\omega'\ k_b(\vec{\omega},\lambda,\vec{\omega}',\lambda')\ k_a(\vec{\omega}',\lambda',\vec{\omega}_0,\lambda_0)\ \frac{1}{|\eta'|}$$

$$\left\{\frac{(1+\mathrm{sgn}\ \eta')}{2}\,\frac{1}{\dfrac{\mu}{|\eta|}+\dfrac{\mu'}{|\eta'|}}+\frac{(1-\mathrm{sgn}\ \eta')}{2}\,\frac{1}{\dfrac{\mu_0}{|\eta_0|}+\dfrac{\mu'}{|\eta'|}}\right\}. \qquad (37)$$

Eqn (37) is valid with all the photon-atom interactions producing a secondary photon. The double scattering processes involving the interactions described in section 2 are shown in figure 2 together with references about their study with this transport model. The total second-order intensity is given by the sum of all the double chain terms, which are n^2 for a total kernel with n single interactions.

4.4. The sum rule for intensities from composite materials

The intensity contributed by a double scattering, described in Eqn (37), is valid for a pure target. The intensity from a composite material is easily obtained from the intensities of the single components if we replace *all the*

a \ b	Photoelectric effect	Coherent scattering (Rayleigh)	Incoherent scattering (Compton)
Photo-electric effect	(P,P) Secondary XRF intensity. Discrete. Eqn (40)	(P,R) XRF photons Rayleigh scattered towards the detector. Discrete. Eqn (46)	(P,C). XRF photons Compton scattered towards the detector. Continuous spectrum. Modifies the XRF line shape. Eqn (48)
Coherent scattering (Rayleigh)	(R,P) XRF due to photoelectric absorption of Rayleigh scattering. Discrete. Eqn (44)	(R,R) Discrete. Modifies the Rayleigh peak. Eqn (51)	(R,C) Continuous spectrum. Modifies the Compton peak. Eqn (55)
Incoherent scattering (Compton)	(C,P) XRF due to photoelectric absorption of Compton scattering. Discrete. Eqn (47)	(C,R) Continuous spectrum. Modifies the Compton peak. Eqn (57)	(C,C) Continuous spectrum. Modifies the Compton peak. Eqn (52)

Figure 2. Physical meaning of the double scattering chains (a, b) involving the photoelectric effect, and Rayleigh and Compton scattering.

attenuation coefficients by mass attenuation coefficients and the kernels by 'mass' kernels in Eqn (37). The following relationship stands for the intensity contributed by the double interaction chain (a,b) in a multielement target

$$I^{(2)}_{(a,b)}(\vec{\omega},\lambda) = \sum_i \sum_j W_i \; W_j \; I^{(2)}_{(a,b)}(\vec{\omega},\lambda)\Big|_{ij} , \qquad (38)$$

where $I^{(2)}_{(a,b)}(\vec{\omega},\lambda)\Big|_{ij}$ is the partial intensity emitted as a consequence of one interaction a on the atom Z_i ('mass' kernel $k_a(\vec{\omega},\lambda,\vec{\omega}',\lambda')\Big|_i$), followed of one interaction b on the atom Z_j ('mass' kernel $k_b(\vec{\omega},\lambda,\vec{\omega}',\lambda')\Big|_j$).

5. MULTIPLE SCATTERING EFFECTS ON THE CHARACTERISTIC LINES

The photoionization process contributes to the X-ray spectrum a number of sharp lines that give qualitative and quantitative information about the elements in the target. X-Ray Fluorescence (XRF), a spectroscopical method of analysis *(57)*, is based on the existing relation between the line intensities and the composition of the specimen. Certainly, this technique requires the knowledge, as detailed as possible, of all the influences that can modify the intensity of the lines and that directly affect the precision of the analysis. On the other hand, the understanding of the changes in the line intensity is necessary to X-ray spectroscopists investigating the atomic parameters involved in the X-ray emission, frequently related to the characteristic lines. The correct prediction of the influence of the experimental conditions on the measurements contributes to an adequate design of both the experiment and the apparatus, improving the quality of the data.

The study of the multiple scattering of the photoelectric effect in XRF gives a clear example of the theoretical approach used for several decades in X-ray spectrometry: the differential intensity (satisfying the Beer-Lambert attenuation law) produced in a differential volume of matter, as a result of one or more interactions, is integrated to obtain the intensity contributed by the process. This approach has two obvious drawbacks. Firstly, with the increase of the multiplicity of scattering, it becomes difficult to write the expression for the differential intensity. Secondly, it is very restrictive in the kind of interactions tractable since it cannot be easily applied to processes with certain complexities like anisotropy.

The first complete deduction of the primary, secondary and tertiary XRF intensities reported by Sherman *(58,59)* was performed with that procedure. A decade later Shiraiwa and Fujino *(60)*, with the same technique, obtained the XRF intensities for polychromatic excitation. These intensities were recently recalculated *(23)* with Eqn (33), and the former expressions were corrected. The fourth-order intensity was also

found *(61)*, showing the validity of transport theory for the analitycal study of higher orders of photoelectric scattering.

The photons scattered by other processes (i.e., the Rayleigh and the Compton effects) also contribute to enhance the XRF intensity, modifying the height of the characteristic lines. In the past, there has been a continued interest in revealing this influence. Several authors attempted a description, with different degrees of detail, and estimated the magnitude of the contribution, from a few percent to more than 30 % of the first-order characteristic line. They used different approaches, from simplistic discussions with a physical basis *(62-64)*, to Monte Carlo simulations *(65,66)*, to models for the diffusion of photons with strong simplification of the scattering cross-sections *(67)*. These results do not give a satisfactory solution to the problem. In contrast, transport theory allows analytical expressions *(38,68)* describing in detail the intensity from one Rayleigh or Compton scattering and one photoelectric collision to be obtained.

The studies of multiple scattering effects on characteristic lines, in the frame of the transport theory, are summarized in the following subsections.

5.1. Chains involving the pure photoelectric effect

The zeroth-order flux - Eqn (27) - is independent of the interaction because it is only related to the source excitation. Therefore, its albedo contribution is zero as may easily be seen.

The first three orders of the XRF intensities can be straightforwardly calculated *(23)* from Eqn (33) and (35)

$$I_{P}^{(1)}(\vec{\omega},\lambda) = \sum_{i} \delta(\lambda-\lambda_i)\, \frac{A(\eta_0,\lambda_0,\eta,\lambda_i)}{4\pi}\, Q_{\lambda_i}(\lambda_0)\, \left[1-\mathcal{U}(\lambda_0-\lambda_{e_i})\right], \qquad (39)$$

$$I_{(P,P)}^{(2)}(\vec{\omega},\lambda) = \sum_{i} \delta(\lambda-\lambda_i)\, \frac{A(\eta_0,\lambda_0,\eta,\lambda_i)}{4\pi}$$

$$\left\{ \sum_{j} \frac{Q_{\lambda_j}(\lambda_0)\, Q_{\lambda_i}(\lambda_j)}{2} \left[1-\mathcal{U}(\lambda_0-\lambda_{e_j})\right] \left[1-\mathcal{U}(\lambda_j-\lambda_{e_i})\right] \right.$$

$$\left. \left\{ \frac{|\eta_0|}{\mu_0} \ell n\left(1+\frac{\mu_0}{\mu_j|\eta_0|}\right) + \frac{|\eta|}{\mu} \ell n\left(1+\frac{\mu}{\mu_j|\eta|}\right) \right\} \right\}, \qquad (40)$$

$$I_{(P,P,P)}^{(3)}(\vec{\omega},\lambda) = \sum_{i} \delta(\lambda-\lambda_i)\, \frac{A(\eta_0,\lambda_0,\eta,\lambda_i)}{4\pi}$$

$$\left\{ \sum_{j}\sum_{k} \frac{Q_{\lambda_k}(\lambda_0)\, Q_{\lambda_j}(\lambda_k)\, Q_{\lambda_i}(\lambda_j)}{4} \right.$$

$$\left[1-\mathcal{U}(\lambda_0-\lambda_{e_k})\right] \left[1-\mathcal{U}(\lambda_k-\lambda_{e_j})\right] \left[1-\mathcal{U}(\lambda_j-\lambda_{e_i})\right]$$

$$\left\{ \frac{|\eta_0|}{\mu_0} \ell n\left(1+\frac{\mu_0}{\mu_k|\eta_0|}\right) \right.$$

$$\left\{ \frac{|\eta_0|}{\mu_0} \ell n\left(1+\frac{\mu_0}{\mu_j|\eta_0|}\right) + \frac{|\eta|}{\mu} \ell n\left(1+\frac{\mu}{\mu_j|\eta|}\right) \right\}$$

$$+ \frac{\eta^2}{\mu^2} \ell n\left(1+\frac{\mu}{\mu_k|\eta|}\right) \ell n\left(1+\frac{\mu}{\mu_j|\eta|}\right)$$

$$+ \frac{1}{\mu_k} \int_0^{\mu_k/\mu_j} \frac{ds}{\frac{\mu_k}{s}+\frac{\mu_0}{|\eta_0|}} \ell n\left(\frac{1+s}{s}\right)$$

$$\left. \left. + \frac{1}{\mu_j} \int_0^{\mu_j/\mu_k} \frac{ds}{\frac{\mu_j}{s}+\frac{\mu}{|\eta|}} \ell n\left(\frac{1+s}{s}\right) \right\} \right\}, \qquad (41)$$

where

$$A(\eta_1,\lambda_1,\eta_2,\lambda_2) = \frac{(1+\operatorname{sgn}\eta_1)}{2}\,\frac{(1-\operatorname{sgn}\eta_2)}{2}\,\frac{I_0}{|\eta_1|}\,\frac{1}{\dfrac{\mu_1}{|\eta_1|}+\dfrac{\mu_2}{|\eta_2|}} \qquad (42)$$

The fourth-order intensity has been calculated *(61)* in similar way, having recourse to the symbolic algebra program MACSYMA *(69)*:

$$I^{(4)}_{(P,P,P,P)}(\vec{\omega},\lambda) = \sum_i \delta(\lambda-\lambda_i)\,\frac{A(\eta_0,\lambda_0,\eta,\lambda_i)}{4\pi}$$

$$\left\{ \sum_j \sum_k \sum_p \frac{Q_{\lambda_p}(\lambda_0)\,Q_{\lambda_k}(\lambda_p)\,Q_{\lambda_j}(\lambda_k)\,Q_{\lambda_i}(\lambda_j)}{8} \right.$$

$$\left[1-\mathcal{U}(\lambda_0-\lambda_{e_p})\right]\left[1-\mathcal{U}(\lambda_p-\lambda_{e_k})\right]\left[1-\mathcal{U}(\lambda_k-\lambda_{e_j})\right]\left[1-\mathcal{U}(\lambda_j-\lambda_{e_i})\right]$$

$$\int_0^1 \frac{d\eta'}{\eta'}\int_0^1 \frac{d\eta''}{\eta''}\int_0^1 \frac{ds}{s}$$

$$\left.\frac{\mathcal{G}(a,a_0,a_i,a',a'')}{(a_i+a)(a_i+a_0)(a'+a)(a'+a_0)(a'+a_i)(a''+a)(a''+a_0)(a''+a_i)(a''+a')}\right\}, \qquad (43)$$

where $a = \mu_i/|\eta|$, $a_0 = \mu_0/|\eta_0|$, $a' = \mu_j/\eta'$, $a'' = \mu_k/\eta''$, $a_i = \mu_p/s$, and the function $\mathcal{G}(a,a_0,a_i,a',a'')$ is a nonreducible polynomial, positive definite, which does not admit factorization in integer powers of its variables.

Since the photoelectric effect is the dominating process in the emission of the characteristic X-rays, the multiple scattering of the pure photoeffect has an important weight in the total intensity. However, its importance can fluctuate very much depending on the absorption properties of the material evaluated at the energies of the participating lines. Besides, a net count of the number of lines contributing to the enhancement is only possible for a given sample and excitation energy. Therefore, the only way to predict the total intensity is by calculating specifically the single order terms with Eqns (39) to (43). The third- and fourth-order contributions could be neglected in low-accuracy computations.

It should be noted that the photoelectric enhancement is even possible in pure targets since characteristic photons can produce photoemission in other series of the same specie of atom. The L lines, for example, receive enhancement from the excited K lines of the same element. This fact should be kept under consideration for measurements of L series parameters.

The angular projections η and η_0 between modulus bars express the azimuthal symmetry of these contributions.

5.2. Chains of mixed interactions involving the photoelectric effect

There are four contributions involving one scattering process and one photoelectric effect. Two of them describe the intensity contributed by coherent and incoherent scattered photons that, absorbed by photoelectric effect, give place to XRF emission. The other two correspond to Rayleigh and Compton scattering of XRF radiation towards the detector. In what follows we shall obtain closed relationships for them, using the results of section 4.

The mathematical complexity in the computation of these intensities depends on whether the involved scattering is Rayleigh or Compton. The Rayleigh scattering contributions are discrete and have the same energy as the characteristic line that they modify. The intensities contributed by the Compton effect, on the contrary, depend on the coupling between the scattering angle and the energy shift, which introduces some difficulties in the computation.

5.2.1. Rayleigh - Photoelectric

The XRF intensity produced by the coherent scattered source-beam is obtained by replacing the kernels k_a and k_b by k_R and k_P respectively in Eqn (37)

$$I^{(2)}_{(R,P)}(\vec{\omega},\lambda) = \delta(\lambda-\lambda_i)\,\frac{A(\eta_0,\lambda_0,\eta,\lambda_i)}{4\pi}\,\frac{\sigma}{Z}\,Q_{\lambda_i}(\lambda_0)\left[1-\mathcal{U}(\lambda_0-\lambda_{e_i})\right]$$

$$\left\{\int_0^{2\pi} d\varphi' \int_0^1 \frac{d\eta'}{\eta'}\,\frac{\left[1+(\vec{\omega}'\cdot\vec{\omega}_0^{(+)})^2\right]}{\frac{\mu_i}{|\eta|}+\frac{\mu_0}{\eta'}}\,F^2(\lambda_0,\vec{\omega}'\cdot\vec{\omega}_0^{(+)},Z) + \right.$$

$$\left.\int_0^{2\pi} d\varphi' \int_0^1 \frac{d\eta'}{\eta'}\,\frac{\left[1+(\vec{\omega}'\cdot\vec{\omega}_0^{(-)})^2\right]}{\frac{\mu_0}{|\eta_0|}+\frac{\mu_0}{\eta'}}\,F^2(\lambda_0,\vec{\omega}'\cdot\vec{\omega}_0^{(-)},Z)\right\}, \qquad (44)$$

where

$$\vec{\omega}_1\cdot\vec{\omega}_2^{(\pm)} = \pm\,\eta_1\eta_2 + \sqrt{1-\eta_1^2}\,\sqrt{1-\eta_2^2}\,\cos(\varphi_1-\varphi_2)\,. \qquad (45)$$

The anisotropy of the Rayleigh scattering is given by the square of the dot product of the direction vectors. The anisotropy in this case is along the direction $\vec{\omega}_0$.

5.2.2. Photoelectric - Rayleigh

The term due to discrete Rayleigh scattering of XRF characteristic photons towards the detector (i.e. in the $\vec{\omega}$ direction) is given by

$$I^{(2)}_{(P,R)}(\vec{\omega},\lambda) = \delta(\lambda-\lambda_i)\,\frac{A(\eta_0,\lambda_0,\eta,\lambda_i)}{4\pi}\,\frac{\sigma}{Z}\,Q_{\lambda_i}(\lambda_0)\left[1-\mathcal{U}(\lambda_0-\lambda_{e_i})\right]$$

$$\left\{\int_0^{2\pi} d\varphi' \int_0^1 \frac{d\eta'}{\eta'}\,\frac{\left[1+(\vec{\omega}'\cdot\vec{\omega}^{(+)})^2\right]}{\frac{\mu_i}{|\eta|}+\frac{\mu_i}{\eta'}}\,F^2(\lambda_i,\vec{\omega}'\cdot\vec{\omega}^{(+)},Z) + \right.$$

$$\left.\int_0^{2\pi} d\varphi' \int_0^1 \frac{d\eta'}{\eta'}\,\frac{\left[1+(\vec{\omega}'\cdot\vec{\omega}^{(-)})^2\right]}{\frac{\mu_0}{|\eta_0|}+\frac{\mu_i}{\eta'}}\,F^2(\lambda_i,\vec{\omega}'\cdot\vec{\omega}^{(-)},Z)\right\}. \qquad (46)$$

Eqn (46) differs from Eqn (44) in that $\vec{\omega}_0$ and λ_0 in the integrals have been replaced by $\vec{\omega}$ and λ_i. Therefore, the anisotropy has been shifted from the incidence to the take-off direction. The change of the wavelength has a more subtle effect since it changes the evaluation points of the mass attenuation coefficients which are complicated functions of λ and Z.

5.2.3. Compton - Photoelectric

The intensity contributed by photoelectric absorption of the incoherent scattered photons of the source is given by

$$I^{(2)}_{(C,P)}(\vec{\omega},\lambda) = \delta(\lambda-\lambda_i)\,\frac{A(\eta_0,\lambda_0,\eta,\lambda_i)}{2\pi}\,\frac{\sigma}{\lambda_C}$$

$$\int_{\lambda_0}^{\lambda_0+2\lambda_c} d\lambda'\; K_{KN}(\lambda',\lambda_0)\,Q_{\lambda_i}(\lambda')\,S(\lambda_0,a',Z)\,[1-\mathcal{U}(\lambda'-\lambda_{e_i})]$$

$$\left\{\int_{\alpha_1'}^{\beta_1'} \frac{d\eta'}{\eta'}\,\frac{\mathcal{U}(\beta_1'-\alpha_1')}{\frac{\mu_i}{|\eta|}+\frac{\mu'}{\eta'}}\,\frac{1}{\sqrt{(1-\eta'^2)(1-\eta_0^2)-(a'-\eta'\eta_0)^2}} + \right.$$

$$\left.\int_{\alpha_2'}^{\beta_2'} \frac{d\eta'}{\eta'}\,\frac{\mathcal{U}(\beta_2'-\alpha_2')}{\frac{\mu_0}{|\eta_0|}+\frac{\mu'}{\eta'}}\,\frac{1}{\sqrt{(1-\eta'^2)(1-\eta_0^2)-(a'+\eta'\eta_0)^2}}\right\}, \qquad (47)$$

where

$$a' = 1 + (\lambda_0-\lambda')/\lambda_C,$$

$$\Delta' = \sqrt{(1-\eta_0^2)(1-a'^2)}\,,$$

$$\alpha_1' = \max(0,a'\eta_0-\Delta'),$$

$$\beta_1' = \min(1,a'\eta_0+\Delta'),$$

$$\alpha_2' = -\min(0,a'\eta_0+\Delta'),$$

and

$$\beta_2' = -\max(-1,a'\eta_0-\Delta').$$

5.2.4. Photoelectric - Compton

The intensity contribution due to XRF photons Compton scattered towards the detector is

$$I^{(2)}_{(P,C)}(\vec{\omega},\lambda) = \frac{A(\eta_0,\lambda_0,\eta,\lambda)}{2\pi}\,\frac{\sigma}{\lambda_C}\,K_{KN}(\lambda,\lambda_i)\,Q_{\lambda_i}(\lambda_0)\left[1-\mathcal{U}(\lambda_0-\lambda_{e_i})\right]$$

$$S(\lambda_i,a,Z)\left\{\int_{\alpha_1}^{\beta_1}\frac{d\eta'}{\eta'}\,\frac{\mathcal{U}(\beta_1-\alpha_1)}{\dfrac{\mu}{|\eta|}+\dfrac{\mu_i}{\eta'}}\,\frac{1}{\sqrt{(1-\eta'^2)(1-\eta^2)-(a-\eta'\eta)^2}}\right.$$

$$\left.+\int_{\alpha_2}^{\beta_2}\frac{d\eta'}{\eta'}\,\frac{\mathcal{U}(\beta_2-\alpha_2)}{\dfrac{\mu_0}{|\eta_0|}+\dfrac{\mu_i}{\eta'}}\,\frac{1}{\sqrt{(1-\eta'^2)(1-\eta^2)-(a+\eta'\eta)^2}}\right\}, \qquad (48)$$

where $a = 1 + (\lambda_i-\lambda)/\lambda_C$, $\Delta = \sqrt{(1-\eta^2)(1-a^2)}$, $\alpha_1 = \max(0, a\eta-\Delta)$, $\beta_1 = \min(1, a\eta+\Delta)$, $\alpha_2 = -\min(0, a\eta+\Delta)$, and $\beta_2 = -\max(-1, a\eta-\Delta)$.

The integration limits in Eqns (47) and (48) cannot exceed the extremes -1 and 1. The Heaviside functions indicate the range of validity of the integrals.

The (P,C) intensity is continuous, in contrast to the contributions (44), (46) and (47) that are discrete. The (P,C) spectrum extends from λ_i to $\lambda_i + 2\lambda_C$ (in energy from $E_i/(1+2E_i/(m_0c^2))$ to E_i).

Eqns (44) to (47) describe the chain contribution of one single line of wavelength λ_i. These corrections must be calculated for every characteristic line in the spectrum. The isotropy of the photoelectric effect makes all the scattering contributions have azimuthal symmetry. For this reason, the intensities are constant along the border of a cone of aperture $\vartheta = \arccos(|\eta|)$ and uniform radius.

5.3. Some examples for single and composite materials

The integrals in the above equations were evaluated numerically with a Romberg algorithm *(70)* to compute the

plotting points in the examples. The outer integrals (when applicable) were calculated with a trapezoidal algorithm over meshes of 20 intervals.

The photoeffect contributions of Eqns (40) and (41), for the Cr Kα line of one alloy specimen, are displayed in figure 3 in units of the first-order intensity of the line, showing the magnitude of the single photoelectric corrections. The second-order is the most important correction over all the range of E_0. It can even exceed the primary intensity under certain conditions. The third-order can achieve a few percent as in the example, while the fourth-order is normally below one percent.

The intensities contributed by scattering are strongly dependent on E_0. The total contribution to the XRF intensity and the single scattering components (relative to the unmodified line) are shown in figures 4(a) to 4(c) for the $K\alpha_1$ lines of Al, Fe and Zr. The energy of the absorption edge marks the start point of the emission in the graphs. The Rayleigh contribution prevails in the region of low energy. The Compton contributions grow monotonically and can achieve an important percent of the line. In practice, however, the coherent

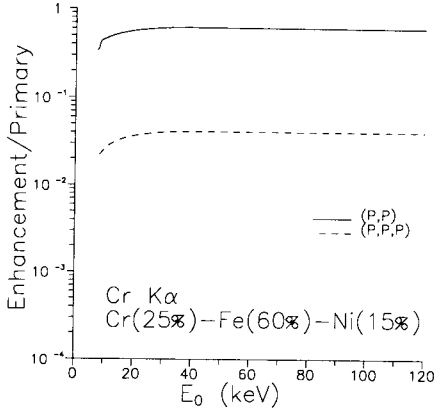

Figure 3. The second- and third-order photoelectric effect contributions to the Cr Kα line shown for the ternary alloy Cr(25 %)-Fe(60 %)-Ni(15 %). The multiple scattering terms, calculated with Eqns. (40) and (41), are plotted in units of first-order intensity (39).

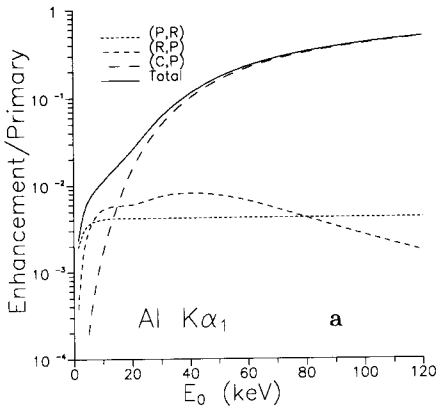

Figure 4.(a) The components of the scattering contribution to the $K\alpha_1$ line (in units of the intensity of the unmodified characteristic line) as a function of the incident beam energy are plotted for Al (from Fernández *(68)*).

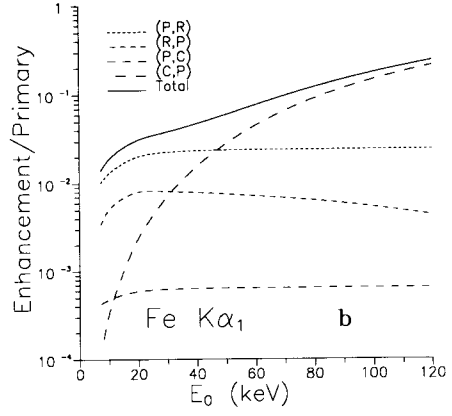

Figure 4.(b) The components of the scattering contribution to the $K\alpha_1$ line (in units of the intensity of the unmodified characteristic line) as a function of the incident beam energy are plotted for Fe (from Fernández *(68)*).

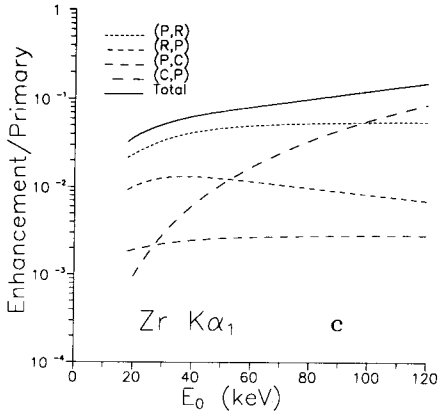

Figure 4.(c) The components of the scattering contribution to the $K\alpha_1$ line (in units of the intensity of the unmodified characteristic line) as a function of the incident beam energy are plotted for Zr (from Fernández *(68)*).

corrections are important for low excitation energy (higher photoelectric probability).

In respect of figure 4, there are no emissions to the left of the K-absorption edge. The total intensity contributed by scattering increases monotonically with the excitation energy. The (P,R) intensity dominates for low E_0, except in a light element like Al. The (C,P) intensity prevails for high E_0. In all the cases the total correction becomes greater for increasing E_0, and is more important in light elements. Note that the scattering contribution in these examples is almost always greater than 1 %.

A lighter matrix favours a greater scattering contribution, as is shown in figure 5. Figure 6 displays the enhancement to the Al $K\alpha_1$ line for a geological specimen as a function of the energy. For E_0 greater than 13 keV the total scattering intensity exceeds the (P,P) correction. Clearly, any attempt to quantify the matrix effects with only the photoelectric enhancement will fail in this sample.

In EDXRF all the lines of the spectrum are produced with the same source of excitation. Lines from different edges will suffer different enhancement by scattering. The greater the separation between E_0 and the absorption edge energy, the

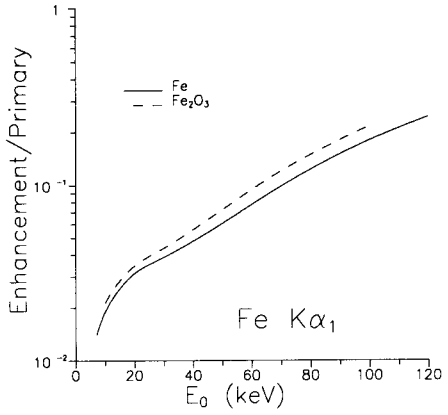

Figure 5. The Fe $K\alpha_1$ line in an iron oxide presenting a higher scattering intensity contribution than in pure iron. The lighter matrix of the oxide favours the scattering (from Fernández *(68)*).

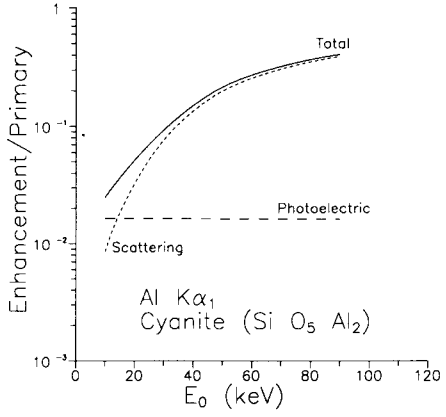

Figure 6. The secondary XRF (P,P) and the scattering enhance ment being the two components of the total second-order intensity. They are plotted between 10 amd 90 keV for the Al $K\alpha_1$ line of a geological sample (Si O_5 Al_2). The scattering contribution is very important in this case and is practically the prevailing enhancement (from Fernández *(68)*).

greater the scattering contribution on the corresponding line. A polychromatic source, a X-ray tube for example, will contribute to the scattering enhancement predominantly in the high energy portion of the spectrum, while the low energy part will contribute through the pure photoeffect.

The (P,C) chain contributes the continuum spectrum exemplified in figure 7. For a given target, the shape of this spectrum varies with E_0, ϑ_0 and ϑ *(68)*. The (P,C) spectrum overlaps the low energy tail of the peak modifying the symmetry of the line. For low and medium Z characteristic lines *(68)* the (P,C) spectrum is too weak to be detected experimentally, although this contribution becomes certainly more important in lines from heavier elements. We guess that this can be the reason for the well known peak asymmetry *(71-73)* in the γ-ray regime.

6. MULTIPLE SCATTERING OF THE RAYLEIGH AND COMPTON EFFECTS

The energy distribution of once incoherently scattered X- and γ-ray photons, the Compton profile, gives valuable information on the momentum distribution of the electrons *(74-76)*. The technique is particularly sensitive to the behaviour of the binding electrons and can be used to test their quantum-mechanical description.

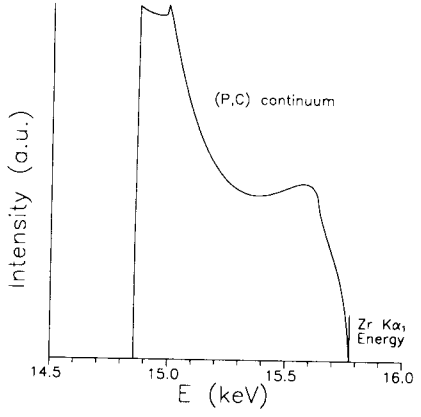

Figure 7. The (P, C) continuous intensity for the Zr $K\alpha_1$ line in a pure Zr sample (E_o = 20 keV, ν_o = 45°, ν = 135°, $\phi = \phi_o$ = 0°).

In measurements, multiple scattered photons contribute a continuous spectrum that overlaps the profile. This interference must be stripped off to obtain acceptable data. Many authors attempted an analytical description of the multiple scattering spectrum using three approaches: the calculation of the scattered electric field *(77,78)*, the integration of a probabilistic differential intensity (as mentioned in section 5) *(79-82)*, and the Boltzmann equation for radiative transfer *(83-86)*. Most of these studies were performed with the first two methods. The approximations in the calculations - geometry, attenuation, and cross-sections - rendered these results qualitative. The few (and old) transport theory applications on this subject were directed to finding general solutions of the Boltzmann equation rather than single terms of multiple scattering.* Since the analytical descriptions were insufficient to correct the profiles *(75,87)*, the spectral distribution of multiple events was calculated with Monte Carlo simulation *(88-90)*.

However, a detailed analytical solution is possible - with Eqn (33) - as has been recently demonstrated *(91)*. In what follows we shall summarize these calculations.

6.1. The Rayleigh and Compton peaks

The first-order contributions due to one single scattering in a pure element target are given by

$$I_R^{(1)}(\vec{\omega},\lambda) = \delta(\lambda-\lambda_0)\,\frac{\sigma}{Z}\,A(\eta_0,\lambda_0,\eta,\lambda_0)\left[1+(\vec{\omega}\cdot\vec{\omega}_0)^2\right]F^2(\lambda_0,\vec{\omega}\cdot\vec{\omega}_0,Z), \qquad (49)$$

$$I_C^{(1)}(\vec{\omega},\lambda) = \delta\left[\lambda_0+\lambda_C(1-\vec{\omega}\cdot\vec{\omega}_0)-\lambda\right]\,\sigma\,K_{KN}(\lambda_0+\lambda_C(1-\vec{\omega}\cdot\vec{\omega}_0),\lambda_0)\,A(\eta_0,\lambda_0,\eta,\lambda_0+\lambda_C(1-\vec{\omega}\cdot\vec{\omega}_0))\,S(\lambda_0,\vec{\omega}\cdot\vec{\omega}_0,Z)\ . \qquad (50)$$

* Curiously, some authors in this field considered, for this reason, that transport theory is unable to separate the multiple-order terms *(87)*.

Eqns (49) and (50) give, respectively, the intensities of the Rayleigh and Compton peaks. Since we neglected the motion of the electrons both peaks are monochromatic for the source and geometry assumed in section 3.

6.2. Chains of double scattering involving the Rayleigh and Compton effects

There are four contributions involving a double scattering with the Rayleigh and the Compton effects: Rayleigh-Rayleigh, Rayleigh-Compton, Compton-Rayleigh, and Compton-Compton. Details for the computations can be found elsewhere *(91)*.

6.2.1. Rayleigh - Rayleigh

This contribution is calculated by substituting the Rayleigh kernel twice into Eqn (37):

$$I_{(R,R)}^{(2)}(\vec{\omega},\lambda) = \delta(\lambda-\lambda_0)\left(\frac{\sigma}{Z}\right)^2 A(\eta_0,\lambda_0,\eta,\lambda_0)$$

$$\left\{\int_0^{2\pi}d\varphi'\int_0^1\frac{d\eta'}{\eta'}\,\frac{\left[1+(\vec{\omega}'\cdot\vec{\omega}^{(+)})^2\right]\left[1+(\vec{\omega}'\cdot\vec{\omega}_0^{(+)})^2\right]}{\frac{\mu_0}{|\eta|}+\frac{\mu_0}{\eta'}}\right.$$

$$F^2(\lambda_0,\vec{\omega}'\cdot\vec{\omega}^{(+)},Z)\,F^2(\lambda_0,\vec{\omega}'\cdot\vec{\omega}_0^{(+)},Z)$$

$$+\int_0^{2\pi}d\varphi'\int_0^1\frac{d\eta'}{\eta'}\,\frac{\left[1+(\vec{\omega}'\cdot\vec{\omega}^{(-)})^2\right]\left[1+(\vec{\omega}'\cdot\vec{\omega}_0^{(-)})^2\right]}{\frac{\mu_0}{|\eta|}+\frac{\mu_0}{\eta'}}$$

$$\left.F^2(\lambda_0,\vec{\omega}'\cdot\vec{\omega}^{(-)},Z)\,F^2(\lambda_0,\vec{\omega}'\cdot\vec{\omega}_0^{(-)},Z)\right\}\ . \qquad (51)$$

The dot products in (51) were defined in (45). The (R,R) intensity overlaps the coherent line (49).

6.2.2. Compton - Compton

The double scattering of the Compton effect is calculated by substituting the Compton kernel (8) twice in Eqn (37):

$$I^{(2)}_{(C,C)}(\vec{\omega},\lambda) = \frac{\sigma^2}{\omega_R \lambda_C} A(\eta_0,\lambda_0,\eta,\lambda)$$

$$\left\{ \int_{\beta_1}^{\gamma_1} \frac{d\eta'}{\eta'} \frac{\mathcal{U}(\gamma_1-\beta_1)}{\sqrt{(1-\eta'^2)(1-\eta_R^2)-(\alpha-\eta'\eta_R)^2}} \right.$$

$$\sum_{k=1}^{2} \frac{K_{KN}(\lambda,\tilde{\lambda}_k^{(+)})\, K_{KN}(\tilde{\lambda}_k^{(+)},\lambda_0)}{\frac{\mu}{|\eta|}+\frac{\mu(\tilde{\lambda}_k^{(+)})}{\eta'}} S(\tilde{\lambda}_k^{(+)},\vec{\omega}\cdot\vec{\omega}_k'^{(+)},Z)\, S(\lambda_0,\vec{\omega}_0\cdot\vec{\omega}_k'^{(+)},Z)$$

$$+ \int_{\beta_2}^{\gamma_2} \frac{d\eta'}{\eta'} \frac{\mathcal{U}(\gamma_2-\beta_2)}{\sqrt{(1-\eta'^2)(1-\eta_R^2)-(\alpha+\eta'\eta_R)^2}}$$

$$\left. \sum_{k=1}^{2} \frac{K_{KN}(\lambda,\tilde{\lambda}_k^{(-)})\, K_{KN}(\tilde{\lambda}_k^{(-)},\lambda_0)}{\frac{\mu}{|\eta|}+\frac{\mu(\tilde{\lambda}_k^{(-)})}{\eta'}} S(\tilde{\lambda}_k^{(-)},\vec{\omega}\cdot\vec{\omega}_k'^{(-)},Z)\, S(\lambda_0,\vec{\omega}_0\cdot\vec{\omega}_k'^{(-)},Z) \right\}, \tag{52}$$

where, for convenience, we have introduced $\beta_1 = \max(0,\alpha\eta_R-D)$, $\gamma_1 = \min(1,\alpha\eta_R+D)$, $\beta_2 = -\min(0,\alpha\eta_R+D)$, $\gamma_2 = -\max(-1,\alpha\eta_R-D)$ and the quantities

$$\tilde{\lambda}_k^{(\pm)} = \lambda_0 + \lambda_C(1-\vec{\omega}_0\cdot\vec{\omega}_k'^{(\pm)}) , \tag{53a}$$

$$\vec{\omega}_0\cdot\vec{\omega}_k'^{(\pm)} = \pm\eta'\eta_0 + \sqrt{1-\eta'^2}\sqrt{1-\eta_0^2}\cos(\varphi_k'^{(\pm)}-\varphi_0) , \tag{53b}$$

$$\vec{\omega}\cdot\vec{\omega}_k'^{(\pm)} = \pm\eta'\eta + \sqrt{1-\eta'^2}\sqrt{1-\eta^2}\cos(\varphi_k'^{(\pm)}-\varphi) , \tag{53c}$$

which are defined in terms of the following functions of η_0, φ_0, λ_0, η, φ, λ, and (the scattering angle) χ

$$\omega_R = |\vec{\omega}+\vec{\omega}_0| = \sqrt{2\,(1+\vec{\omega}\cdot\vec{\omega}_0)} = 2\cos\frac{\chi}{2} , \tag{54a}$$

$$\alpha = \frac{1}{\omega_R}\left(2+\frac{\lambda_0-\lambda}{\lambda_C}\right) , \tag{54b}$$

$$\eta_R = \frac{\eta+\eta_0}{\omega_R} , \tag{54c}$$

$$\varphi_R = \arccos\left(\frac{\sqrt{1-\eta_0^2}+\sqrt{1-\eta^2}\cos\varphi}{\sqrt{\omega_R^2-(\eta_0-\eta)^2}}\right) , \tag{54d}$$

$$D = \sqrt{(1-\eta_R^2)(1-\alpha^2)} , \tag{54e}$$

$$\varphi_1'^{(\pm)} = \varphi_R + \arccos\left(\frac{\alpha\mp\eta'\eta_R}{\sqrt{(1-\eta'^2)(1-\eta_R^2)}}\right) , \tag{54f}$$

$$\varphi_2'^{(\pm)} = 2\pi + \varphi_R - (\varphi_1'^{(\pm)}-\varphi_R) . \tag{54g}$$

The integration limits β_i and γ_i cannot exceed the values -1 and 1. The Heaviside functions in the integrals are different from zero only when $\gamma_i > \beta_i$ and indicate the validity range of every integral. The (C,C) intensity is continuous, in contrast to the preceding contribution. Its wavelength spectrum extends from $\lambda_0+\lambda_C(2-\omega_R)$ to $\lambda_0+\lambda_C(2+\omega_R)$ and has the characteristic shape shown in figure 8. Eqn (52) is valid for $\omega_R \neq 0$, $\alpha^2 \neq 1$ and $\eta_R^2 \neq 1$. Limit cases for the special values of ω_R, η_R and α can be calculated similarly.

6.2.3. Rayleigh - Compton

The contribution of Compton scattering of Rayleigh scattered photons is obtained similarly to Eqn (52)

$$I^{(2)}_{(R,C)}(\vec{\omega},\lambda) = \frac{\sigma^2}{Z\,\lambda_C} A(\eta_0,\lambda_0,\eta,\lambda)\, K_{KN}(\lambda,\lambda_0)\, S(\lambda_0,a,Z)$$

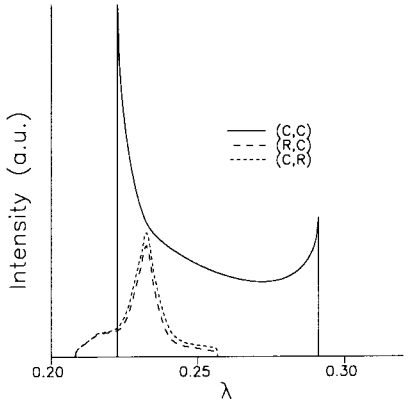

Figure 8. Characteristic shape of the double scattering continuous contributions due to the combined influence of the Compton and Rayleigh effects. Calculations are for Al excited with 59.54 keV (γ line of ^{241}Am) and for the geometry defined by the incidence and take-off polar angles ν_o/ν = 45°/135°. Azimuthal angles ϕ_o/ϕ will be assumed as 0°/0° unless expressly indicated.

$$\left\{ \int_{\beta_1}^{\gamma_1} \frac{d\eta'}{\eta'} \frac{1}{\dfrac{\mu}{|\eta|} + \dfrac{\mu_0}{\eta'}} \frac{\mathcal{U}(\gamma_1 - \beta_1)}{\sqrt{(1-\eta'^2)(1-\eta^2) - (a-\eta'\eta)^2}} \right.$$

$$\sum_{k=1}^{2} \left(1 + (\vec{\omega}_0 \cdot \vec{\omega}_k'^{(+)})^2\right) F^2(\lambda_0, \vec{\omega}_0 \cdot \vec{\omega}_k'^{(+)}, Z)$$

$$+ \int_{\beta_2}^{\gamma_2} \frac{d\eta'}{\eta'} \frac{1}{\dfrac{\mu_0}{|\eta_0|} + \dfrac{\mu_0}{\eta'}} \frac{\mathcal{U}(\gamma_2 - \beta_2)}{\sqrt{(1-\eta'^2)(1-\eta^2) - (a+\eta'\eta)^2}}$$

$$\left. \sum_{k=1}^{2} \left(1 + (\vec{\omega}_0 \cdot \vec{\omega}_k'^{(-)})^2\right) F^2(\lambda_0, \vec{\omega}_0 \cdot \vec{\omega}_k'^{(-)}, Z) \right\} , \qquad (55)$$

where $\beta_1 = \max(0, a\eta - D)$, $\gamma_1 = \min(1, a\eta + D)$, $\beta_2 = -\min(0, a\eta + D)$, $\gamma_2 = -\max(-1, a\eta - D)$ and $\vec{\omega}_0 \cdot \vec{\omega}_k'^{(\pm)}$ - as in Eqn (53b) - are defined

in terms of

$$a = 1 + \frac{\lambda_0 - \lambda}{\lambda_C} , \qquad (56a)$$

$$D = \sqrt{(1-\eta^2)(1-a^2)} , \qquad (56b)$$

$$\varphi_1'^{(\pm)} = \varphi + \arccos\left(\frac{a \mp \eta'\eta}{\sqrt{(1-\eta'^2)(1-\eta^2)}} \right) , \text{ and} \qquad (56c)$$

$$\varphi_2'^{(\pm)} = 2\pi + \varphi - (\varphi_1'^{(\pm)} - \varphi) . \qquad (56d)$$

The meaning of the limits β_i and γ_i is as in Eqn (52). The (R,C) intensity is continuous and its wavelength spectrum extends from λ_0 to $\lambda_0 + 2\lambda_C$ (in energy from $E_0/(1+2E_0/(m_0c^2))$ to E_0); therefore it overlaps partially the (C,C) spectrum. The shape of the (R,C) spectrum is shown in figure 8. The characteristic maximum at the energy of the Compton line broadens that peak.

6.2.4. Compton - Rayleigh

The Rayleigh scattering of Compton scattered photons is obtained similarly

$$I_{(C,R)}^{(2)}(\vec{\omega}, \lambda) = \frac{\sigma^2}{Z\,\lambda_C} A(\eta_0, \lambda_0, \eta, \lambda)\, K_{KN}(\lambda, \lambda_0)\, S(\lambda_0, a, Z)$$

$$\left\{ \int_{\beta_1}^{\gamma_1} \frac{d\eta'}{\eta'} \frac{1}{\dfrac{\mu}{|\eta|} + \dfrac{\mu}{\eta'}} \frac{\mathcal{U}(\gamma_1 - \beta_1)}{\sqrt{(1-\eta'^2)(1-\eta_0^2) - (a-\eta'\eta_0)^2}} \right.$$

$$\sum_{k=1}^{2} \left(1 + (\vec{\omega} \cdot \vec{\omega}_k'^{(+)})^2\right) F^2(\lambda, \vec{\omega} \cdot \vec{\omega}_k'^{(+)}, Z)$$

$$+ \int_{\beta_2}^{\gamma_2} \frac{d\eta'}{\eta'} \frac{1}{\dfrac{\mu_0}{|\eta_0|} + \dfrac{\mu}{\eta'}} \frac{\mathcal{U}(\gamma_2 - \beta_2)}{\sqrt{(1-\eta'^2)(1-\eta_0^2) - (a+\eta'\eta_0)^2}}$$

$$\sum_{k=1}^{2} \left[1 + (\vec{\omega}\cdot\vec{\omega}'^{(-)}_k)^2 \right] F^2(\lambda, \vec{\omega}\cdot\vec{\omega}'^{(-)}_k, Z) \Bigg\} , \qquad (57)$$

where $\beta_1 = \max(0, a\eta_0 - D)$, $\gamma_1 = \min(1, a\eta_0 + D)$, $\beta_2 = -\min(0, a\eta_0 + D)$, $\gamma_2 = -\max(-1, a\eta_0 - D)$, and $\vec{\omega}\cdot\vec{\omega}'^{(\pm)}_k$ - as in Eqn (53c) - are defined in terms of

$$a = 1 + \frac{\lambda_0 - \lambda}{\lambda_C} , \qquad (58a)$$

$$D = \sqrt{(1 - \eta_0^2)(1 - a^2)} , \qquad (58b)$$

$$\varphi'^{(\pm)}_1 = \varphi_0 + \arccos\left(\frac{a \mp \eta' \eta_0}{\sqrt{(1 - \eta'^2)(1 - \eta_0^2)}} \right) , \text{ and} \qquad (58c)$$

$$\varphi'^{(\pm)}_2 = 2\pi + \varphi_0 - (\varphi'^{(\pm)}_1 - \varphi_0) . \qquad (58d)$$

The meaning of the limits β_i and γ_i is as in the preceding equation. The (C,R) intensity is continuous and its wavelength spectrum extends from λ_0 to $\lambda_0 + 2\lambda_C$ (as in the preceding case). Therefore, it overlaps partially the (C,C) and fully the (R,C)

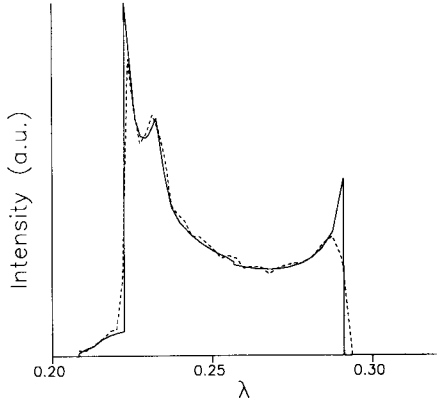

Figure 9. Analytical prediction (solid line) of a second-order spectrum compared to a 50,000 histories MC simulation *(92)* (dashed line) under the same conditions assumed in sections 2 and 3. The target is A1 excited with 59.54 keV at 45°/135°/0°.

spectra. The shape of the (C,R) spectrum is similar but not equal to that of (R,C) as shown in figure 8.

6.3. Monte Carlo simulation and higher orders of scattering

The above analytical results were checked with a Monte Carlo simulation *(92)* reproducing the same physical problem described in sections 2 and 3. The predicted MC spectrum match closely the analytical one, as is shown in figure 9.

The figure shows three 'peaks', well differentiated. Two of them belong to the extremes of the (C,C) distribution, and the central one is the peaked distribution due to the sum of the (C,R) plus the (R,C) intensities whose maximum coincides with the Compton peak wavelength. Depending on the target, the excitation wavelength, and the geometry, the three peaks can look like two, or like only one.

Since analytical expressions are still not available for the third- and fourth-order components, they were simulated with Monte Carlo. Figure 10 displays the spectra for O, Al and Cu. With regard to the figure, higher order scattering becomes more important for light elements as can be appreciated (the heights of the plots are in scale 1:20:40 for decreasing atomic number). Another element of quantification is the height of the coherent line (near the right side in the plots) that becomes more important for increasing Z. For low Z, third- and fourth-order contributions cannot be neglected. The results shown that multiple scattering with only the Compton effect is the most important term in every case. These contributions are very important in light elements, but can be safely neglected in the medium Z range.

6.4. Some examples for pure targets

Under the assumptions of this work, the first-order Compton term gives a monochromatic line, whereas the multiple-order terms with the Compton effect contribute continuous spectra. Therefore, the terms of the Neumann series can be associated with different shapes in the spectrum, having an almost identical experimental manifestation. This fact supports the validity of the iterative approach applied in section 4.

Figure 11 shows the behaviour of the Compton intensity, the total double scattering intensity under the Compton peak,

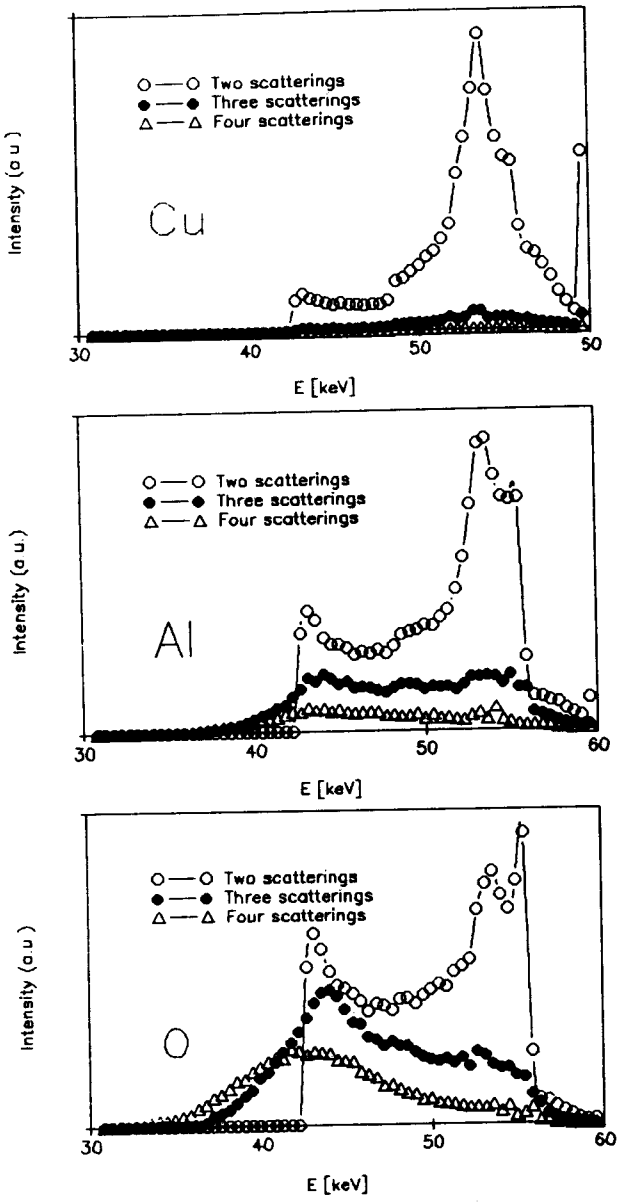

Figure 10. Two-, three- and four-collision total intensities simulated with MC *(92)* for three elements excited with the same energy E_o = 59.54 keV.

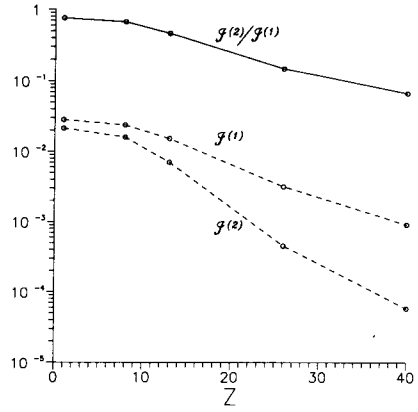

Figure 11. The single and double scattering integrated intensities describing the overall contribution of the corresponding order of scattering.
Here they are plotted as a function of the atomic number Z of the target for some representative elements (H, O, Al, Fe, Zr), polar angles of 45°/135° and an excitation of 59.54 keV. The double-to-single-intensity ratio $\tau^{(2)}/\tau^{(1)}$ that gives the importance of the continuous second order ((C,C)+(C,R)+(R,C)) relative to the intensity of the Compton peak is plotted as a solid line.

and its ratio as a function of Z. The ratio vanishes for increasing Z, rendering cleaner the Compton peak. For low Z, double scattering can be high (> 70% of the Compton peak for H) and, therefore, higher orders of multiple scattering should be calculated.

Figure 12 displays the single terms of double scattering as a function of Z. The (C,C) term decreases monotonically, whereas the mixed scattering terms, (R,C) and (C,R), reach a maximum (near Al) and decrease with lower slope than (C,C). The different slopes allow a similar contribution of the three components near Fe. For elements lighter than Fe the (C,C) intensity dominates. For heavier elements the mixed components become higher than (C,C), their peaked shape producing a greater distortion of the Compton profile.

The excitation wavelength λ_0 (energy E_0) determines the position of the intervals for both the attenuation of the beam into the target and the next scattering. Figure 13 shows how the increase of E_0 has the effect of increasing the integral

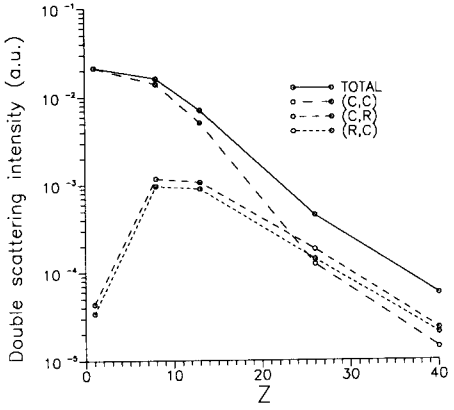

Figure 12. Partial double scattering intensities as a function of the atomic number Z. The (C,C), (C,R) and (R,C) continuous contributions are plotted as dashed line. The total double scattering is plotted with a solid line. Angles are 45°/135°/0° and energy is 59.54 keV.

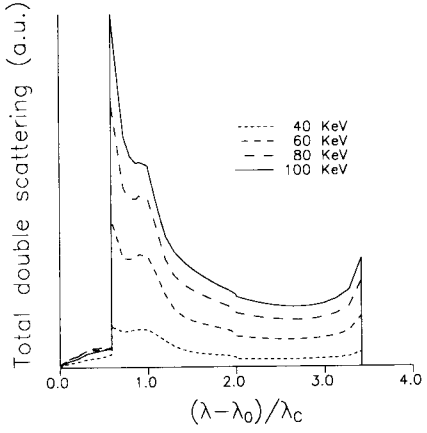

Figure 13. Total double scattering in Al as a function of the ratio $(\lambda-\lambda_o)/\lambda_c$ for several incidence energies E_o. The incidence and take-off angles are 45° and 135° respectively.

intensity without modifying the wavelength width (but shifting the wavelength origin) of the spectrum.

Although the angular coordinates ϑ, ϑ_0 and $\varphi-\varphi_0$ (or the scattering angle χ) modify the shape of the spectrum, it is difficult to establish a general behaviour beyond the following properties *(91)*. The angle χ defines the width of the continuous wavelength spectrum in the (C,C) case. A change in ϑ_0 and ϑ maintaining χ fixed varies the relative contribution of the partial second-order intensities to the double scattering spectrum, and modifies the shape of the (C,C) intensity. Since χ is constant, the wavelength limits of the spectra remain unchanged. The spectrum becomes narrower for increasing ϑ. The increase of χ produces the concentration of the spectrum at the energy of the Compton peak.

6.5. Comparison with experimental data

In order to compare this theory with experimental data, a full spectrum for water was built by joining both the monochromatic and the multiple scattering continuous parts. The first- and second-order contributions were calculated with the computer program SHAPE *(93)* using the analytical expressions

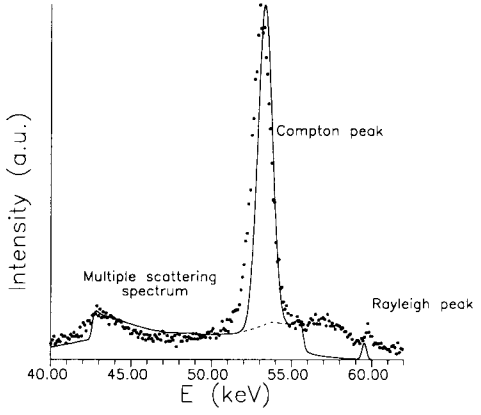

Figure 14. X-ray spectrum of H_2O excited with the 59.54 keV line. Geometry is 45°/135°/0°. The solid line represents the theoretical estimation computed with SHAPE *(93)* and corrected with the third and fourth order contributions calculated with MC *(92)*. Circles denote experimental data (courtesy of R. Sartori, FaMAF, University of Córdoba).

described in this work. The third- and fourth-order components were determined with MC simulation. The monochromatic peaks were artificially broadened with a Gaussian shape to improve the fit of the whole spectrum. The multiple scattering orders are not retouched. The spectrum so obtained matches well experimental points as is shown in figure 14. The dashed line identifies the multiple scattering contribution. As can be appreciated, multiple scattering introduces low deformation for this geometry.

7. SUMMARY

The multiple scattering of photons is important in X-ray spectrometry where a precise knowledge of the X-ray spectrum is mandatory. Entire portions of the continuum spectrum and strong changes in the intensity of the lines are due to multiple scattering. This effect becomes more important in reflection experiments on targets of infinite optical thickness, suitable to achieve the higher counting rates.

Transport theory has been revealed as adequate in obtaining, analytically, the intensities contributed by the the processes described in section 2 - the photoelectric effect, the Rayleigh, and the Compton scattering -, in a multiple-collision scheme. The multiple-orders solution of the Boltzmann equation - deduced in section 4 - allows the contribution of single chains of interactions in the spectrum to be identified, and allows their influence to be optimized. Some of these contributions have been explained with this approach for the first time. Others, studied previously with different techniques, have been included in a wide explanation which can be extended to other geometries, or to other properties of the radiation, as for example, the polarization of photons. The method has deep conceptual similarities with the Monte Carlo simulation of Markovian chains, but remains an expression of the classical theory of diffusion that gives understandable results in analytical way.

As we saw, the first-order contributions of the three processes are discrete, i.e., peaks. Multiple scattering modifies them in different ways. The characteristic lines suffer both a discrete and a continuous enhancement. Their intensities increase and their shapes change, revealing a low-energy tail in the peaks, as was shown in section 5. The Rayleigh line changes only the intensity, whereas the Compton line suffers the overlapping of a very intense continuous spectrum (section 6).

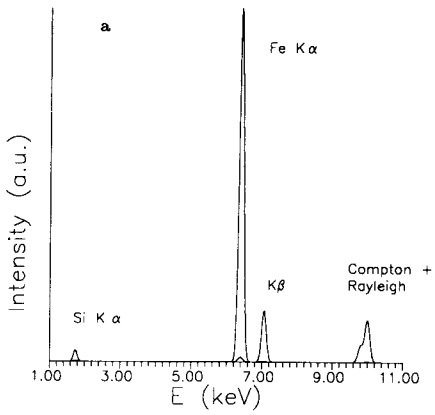

Figure 15.(a) EDXRF spectra of SiO_2(90 %)-Fe_2O_3 (10 %) in geometry of 45°/135°/0°. Full spectrum for excitation with a 10 keV source. The solid line in the bottom corresponds to the multiple scattering spectrum (from Fernández and Sumini *(93)*).

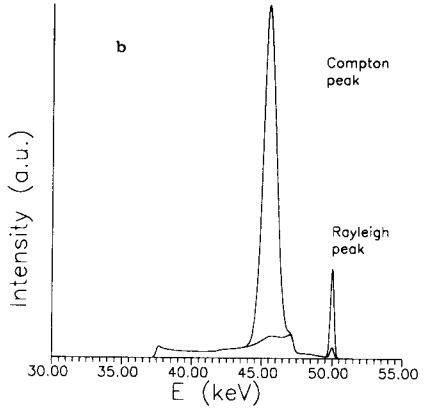

Figure 15.(b) EDXRF spectra of SiO_2(90)-Fe_2O_3 (10 %) in geometry of 45°/135°/0°. Detail of the Compton and Rayleigh peaks for excitation with 50 keV photons. The solid line in the bottom corresponds to the multiple scattering spectrum (from Fernández and Sumini *(93)*).

The superposition of the multiple scattering effects and the lines gives the whole X-ray spectrum, which can be very complex for composite materials. In order to understand better the contributions from single chains of multiple collisions, the computer code SHAPE *(93)* has been developed. It computes all the first-, and second-order intensities, plus the third-order (P,P,P) term, building up quite a detailed wavelength spectrum for any target composition, excitation wavelength spectrum and geometrical set-up. This spectrum is transformed to energy and geometrical set-up. This spectrum is transformed to the energy domain and is modified according to a solid state detector response *(94-98)* to match better real measurements. Figure 15 illustrates an EDXRF spectrum for a geological specimen. Computations agree well with experimental data in the range of energy 1-100 keV confirming the validity of the adopted scheme.

Performed calculations allow us to foresee that all the multiple-scattering terms will vanish if the propagation plane *(99)* - the plane containing both beam directions - is tilted at 90°, providing a means to recover the first-order contributions without the interference of the multiple collision spectrum.

Interest in photon spectroscopy calculations will increase in the future if polarization effects, electron motion, and electron-photon processes are included in the theory. With this improvement, the X-ray spectra could be calculated with a degree of detail which is still difficult to obtain today with the bigger programs of MC simulation. Furthermore, there would be deterministic accuracy, less time consumption, and a better understanding.

NOMENCLATURE

A	atomic weight,
E	energy of photons,
$F(\lambda', \vec{\omega}\cdot\vec{\omega}', Z)$	coherent atomic form factor for an atom with atomic number Z,
$f(\vec{r},\vec{\omega},\lambda)$	angular flux,
$f^{(n)}(z,\vec{\omega},\lambda)$	angular flux of n-th order, i.e. the angular flux due to n interactions in the medium,
$\mathcal{F}[f]$	Fourier transform of the function f,

$\tilde{f}$	Fourier transform of the function f,
h	Planck constant,
I_0	constant intensity of the source,
$\hat{I}$	integral operator in Eqn (18) $(=\int_0^{\infty} d\lambda' \int_{4\pi} d\omega')$,
$I^{(n)}(\vec{\omega},\lambda)$	angular intensity of n-th order,
$\mathfrak{I}^{(n)}(\vec{\omega})$	wavelength-integrated angular intensity of n-th order,
$I_a^{(1)}(\vec{\omega},\lambda)$	first-order intensity due to the interaction a,
$I_{(a,b)}^{(2)}(\vec{\omega},\lambda)$	second-order intensity (corresponding to the chain of interactions a and b, in this order),
$I_{(a,b)}^{(2)}(\vec{\omega},\lambda)\Big\|_{ij}$	second-order intensity of the photons produced as a consequence of one interaction a on the atom Z_i followed of one interaction b on the atom Z_j^i,
$I_{(P,P,P)}^{(3)}(\vec{\omega},\lambda)$	third-order intensity due to three successive photoelectric interactions,
$I_{(P,P,P,P)}^{(4)}(\vec{\omega},\lambda)$	fourth-order intensity due to four successive photoelectric interactions,
J_{λ_i}	absorption-edge jump,
$k_a(\vec{\omega},\lambda,\vec{\omega}',\lambda')$	interaction kernel describing the probability density (per unit path, per unit solid angle, per unit wavelength) that the process a can change the phase-space variables $\vec{\omega}',\lambda'$ to $\vec{\omega},\lambda$,
$k_a(\vec{\omega},\lambda,\vec{\omega}',\lambda')\Big\|_j$	'mass' kernel for the interaction a with the species of atoms Z_j,
$K_{KN}(\lambda,\lambda')$	Klein-Nishina factor,
$\hat{K}$	integral operator $(=\frac{1}{\pi}\int_{-\infty}^{\infty}\frac{d\tau}{(q-\tau)})$,

N	Avogadro's number,
$\mathbb{P}$	projection operator,
$Q_{\lambda_i}(\lambda)$	radiative photoelectric attenuation coefficient for the emission of the line at λ_i,
r_0	classical radius of the electron,
$\mathcal{S}(\vec{r},\vec{\omega},\lambda)$	source term,
$S(\lambda',\vec{\omega}\cdot\vec{\omega}',Z)$	incoherent scattering function for an atom with atomic number Z,
sgn z	sign function,
$\mathcal{U}(x-a)$	Heaviside (unitary step) function,
W_j	weight fraction of element j in the sample,
Z	atomic number,
χ	scattering angle,
$\delta(x-a)$	Dirac δ-function,
δ_{n0}	Kronecker δ-function,
η	(= cos ϑ) director cosine ω_z,
Γ_{λ_i}	line emission probability of the line at λ_i into its own spectral series,
λ	wavelength of the emitted photons,
λ_0	wavelength of the monochromatic source beam,
λ_i	wavelength of the characteristic line i,
λ_C	Compton wavelength,
μ	total attenuation coefficient obtained by adding the attenuation coefficients for the dominating processes in the X-ray regime (see Eqn (3)),

μ_0	(= $\mu(\lambda_0)$),
μ_i	(= $\mu(\lambda_i)$),
$(\mu/\rho)_j$	total mass attenuation coefficient for the single element j,
ν	frequency,
$\vec{\omega}$	unitary vector oriented in the take-off direction,
$\vec{\omega}_0$	unitary vector oriented in the incidence direction,
$d\omega$	differential of solid angle in the direction $\vec{\omega}$ (= $d\eta d\varphi$),
ω_{λ_i}	fluorescence yield of the line at λ_i,
ρ	density,
σ	(= $\frac{r_0^2\,\rho N Z}{2\,A}$) macroscopic scattering coefficient,
σ_C	Compton scattering attenuation coefficient,
σ_R	Rayleigh scattering attenuation coefficient,
$\sigma_T(\lambda',\vec{\omega}')$	integrated cross-section for the process T obtained by integrating the kernel (Eqn (2)),
ϑ	take-off polar angle,
ϑ_0	incidence polar angle,
τ	photoelectric effect attenuation coefficient,
$\tau_s(\lambda)$	photoelectric attenuation coefficient of the emitter element s at the wavelength λ,
$\otimes$	convolution product,
∇	gradient operator,

SUBSCRIPTS

C	Compton scattering
P	photoelectric effect
R	Rayleigh scattering

REFERENCES

1. R.D. Evans, "The Atomic Nucleus," McGraw-Hill, New York (1955).

2. B.K. Agarwal, "X-Ray Spectroscopy," Springer-Verlag, Berlin (1979).

3. J.M. Jauch and F. Rohrlich, "The Theory of Photons and Electrons," Springer-Verlag, Berlin (1976).

4. C.M. Davisson and R.D. Evans, Gamma-ray absorption coefficients, Rev. Mod. Phys. 24, 79-107 (1952).

5. J.H. Hubbell, W.H. McMaster, N. Kerr del Grande and J.H. Mallett, X-ray cross-sections and attenuation coefficients, in "International Tables for X-Ray Crystallography" (J.A. Ibers and W.C. Hamilton, ed.) Vol 4, pp. 47-70, Kynoch Press, Birmingham (1974).

6. D.C. Creagh, The resolution of discrepancies in tables of photon attenuation coefficients, Nucl. Instr. Meth. in Phys. Res. A 255, 1-16 (1987).

7. N.G. Alexandropoulos, T. Chatzigeogiou, G. Evangelakis, M.J. Cooper and S. Manninen, Bremsstrahlung and its contributions to the gamma ray spectra of solids, Nucl. Instr. Meth. in Phys. Res. A 271, 543-545 (1988).

8. C. Bui and M. Milazzo, Measurements of anomalous dispersion in Rayleigh scattering of characteristic X-ray fluorescence, N. Cimento D 11, 655-686 (1989).

9. W.H. McMaster, N. Kerr del Grande, J.H. Mallett and J. Hubbell, Compilation of X-ray cross-sections, Lawrence Livermore National Laboratory Report UCRL-50174, Sect. 2, Rev. 1 (1969).

10. E. Storm and H.I. Israel, Photon cross-sections from 1 keV to 100 MeV for elements Z=1 to Z=100, Nucl. Data Tables A 7, 565-681 (1970).

11. W.J. Veigele, Photon cross-sections from 0.1 keV to 1 MeV for elements Z=1 to Z=94, Atomic Data 5, 51-111 (1973).

12. J.H. Hubbell, H.M. Gerstemberg and E.B. Saloman, Bibliography of photon total cross-section (attenuation coefficient) measurements 10 eV to 13.5 GeV, National Bureau of Standards Report NBSIR 86-3461 (1986).

13. E.B. Saloman, J.H. Hubbell and J.H. Scofield, X-ray attenuation cross-sections for energies 100 eV to 100 keV and elements Z=1 to Z=92, At. Data Nucl. Data Tables 38, 1-197 (1988).

14. D.E. Cullen, M.H. Chen, J.H. Hubbell, S.T. Perkins, E.F. Plechaty, J.A. Rathkopf and J.H. Scofield, Tables and graphs of photon-interaction cross-sections from 10 eV to 100 GeV derived from the LLNL evaluated photon data library (EPDL), Lawrence Livermore National Laboratory Report UCRL-50400, Vol 6, Parts A and B, Rev. 4 (1989).

15. L. Kissel and R.H. Pratt, Status of cross-section data for photon scattering of atoms, Trans. Am. Nucl. Soc. 55, 199-200 (1987).

16. R. Ribberfors and K.F. Berggren, Incoherent-X-ray-scattering functions and cross-sections $(d\sigma/d\Omega')_{incoh}$ by means of a pocket calculator, Phys. Rev A 26, 3325-3333 (1982); Erratum, Phys. Rev. A 29, 3451 (1984).

17. U. Fano and J.W. Cooper, Spectral distribution of atomic oscillator strengths, Rev. Mod. Phys. 40, 441-507 (1968).

18. A.F. Starace, Theory of atomic photoionization, in "Handbuch der Physik" (W. Melhorn, ed.) Vol XXXI, pp. 1-121, Springer-Verlag, Berlin (1982).

19. J.H. Scofield, Status of atomic photoeffect cross-section data, Trans. Am. Nucl. Soc. 55, 200-201 (1987).

20. J.H. Scofield, Theoretical photoionization cross-sections from 1 to 1500 keV, Lawrence Livermore National Laboratory Report UCRL-51326 (1973).

21. J.A. Bearden, X-ray wavelengths, Rev. Mod. Phys. 39, 78-124 (1967).

22. J.A. Bearden and A.F. Burr, Reevaluation of X-ray atomic energy levels, Rev. Mod. Phys. 39, 125-142 (1967).

23. J.E. Fernández, XRF intensity in the frame of the transport theory, X-Ray Spectrom. 18, 271-279 (1989).

24. M.O. Krause and J.H. Oliver, Natural widths of atomic K and L levels, Kα X-ray lines and several KLL Auger lines, J. Phys. Chem. Ref. Data 8, 329-338 (1979).

25. S.I. Salem, F. Boehm and P.L. Lee, Instrumental line width of a bent crystal spectrometer and measurement of the Kβ X-ray width, Nucl. Instr. Meth. 140, 511-514 (1977).

26. R.W. Fink, R.C. Jopson, H. Mark and C.D. Swift, Atomic fluorescence yields, Rev. Mod. Phys. 38, 513-540 (1966).

27. W. Bambynek, B. Crasemann, R.W. Fink, H.U. Freund and M. Mark. X-ray fluorescence yields, Auger, and Koster-Kronig transition probabilities, Rev. Mod. Phys. 44, 716-813 (1972).

28. M.O. Krause, Atomic radiative and radiationless yields for K and L shells, J. Phys. Chem. Data 8, 307-327 (1979).

29. A. Langemberg and J. Van Eck, An evaluation of K-shell fluorescence yields; observation of outer-shell effects, J. Phys. B 12, 1331-1350 (1979).

30. D.D. Cohen, Average L shell fluorescence yields, Nucl. Instr. and Meth. in Phys. Res. B 22, 55-58 (1987).

31. John H. Hubbell, Bibliography and current status of K, L, and higher shell fluorescence yields for computation of photon energy-absorption coefficients, National Institute of Standards and Technology Report NISTR 89-4144 (1989).

32. J.H. Scofield, Radiative decay rates of vacancies in the K and L shells, Phys. Rev. 179, 9-16 (1969).

33. J.H. Scofield, Exchange corrections of K X-ray emission rates, Phys. Rev. A 9, 1041-1049 (1974).

34. J.S. Hansen, H.U. Freund and R.W. Fink, Radiative X-ray transition probabilities to the K-shell, Nucl. Phys. A 142, 604-608 (1970).

35. S.I. Salem, S.L. Panossian and R.A. Krause, Experimental K and L relative X-ray emission rates, At. Data Nucl. Data Tables 14, 91-109 (1974).

36. M.R. Khan and M. Karimi, Kβ/Kα ratios in energy dispersive X-ray emission analysis, X-Ray Spectrom. 9, 32-35 (1980).

37. P.P. Kane, L. Kissel, R.H. Pratt and S.C. Roy, Elastic scattering of γ-rays and X-rays by atoms, Phys. Rep. 140, 75-159 (1986).

38. J.E. Fernández, V.G. Molinari and M. Sumini, Corrections for the effect of scattering on XRF intensity, in "Advances in X-Ray Analysis" (C.S. Barrett et al., ed.) Vol. 33, pp. 553-566, Plenum Press, New York (1990).

39. J.H. Hubbell, W.J. Veigele, E.A. Briggs, R.T. Brown, D.T. Cromer and R.J. Howerton, Atomic form factors, incoherent scattering functions, and photon scattering cross-sections, J. Phys. Chem. Ref. Data 4, 471-538 (1975); Erratum, J. Phys. Chem. Ref. Data 6, 615-616 (1977).

40. J.H. Hubbell and I. Øverbø, Relativistic atomic form factors and photon coherent scattering cross-sections, J. Phys. Chem. Ref. Data 8, 69-105 (1979).

41. D. Schaupp, M. Schumacher, F. Smend and P. Rullhusen, and J.H. Hubbell Small-angle Rayleigh scattering of photons at high energies: Tabulation of relativistic HFS modified atomic form factors, J. Phys. Chem. Ref. Data 12, 467-512 (1983).

42. W.J. Veigele, P.T. Tracy and E.M. Henry, Compton effect and electron binding, Am. J. Phys. 34, 1116-1121 (1966).

43. D.T. Cromer and J.T. Waber, Atomic scattering factors for X-rays, in "International Tables for X-Ray Crystallography" (J.A. Ibers and W.C. Hamilton, ed.) Vol 4, pp. 71-147, Kynoch Press, Birmingham (1974).

44. A.H. Compton, A quantum theory of the scattering of X-rays by light elements, Phys. Rev. 21, 483-502 (1923).

45. R.D. Evans, Compton effect, in "Handbuch der Physik" (S. Flugge, ed.) Vol XXXIV, pp. 218-298, Springer, Berlin (1958).

46. O. Klein and Y. Nishina, Über die streuung von strahlung durch freie elektronen nach der neuen relativistischen quantendynamik von Dirac, Z. Phys. 52, 853-868 (1929).

47. V.H. Smith Jr, A.J. Thakkar and D.C. Chapman, A new analytical approximation to atomic incoherent X-ray scattering intensities, Acta Cryst. A 31, 391-392 (1975).

48. G.C. Pomraning, "The equations of radiation hydrodynamics," Pergamon Press, Oxford (1973).

49. U. Fano, L.V. Spencer and M.J. Berger, Penetration and diffusion of X-rays, in "Handbuch der Physik" (S. Flugge, ed.) vol XXXVIII/2, pp. 660-817, Springer, Berlin (1960).

50. J.E. Fernández, V.G. Molinari and M. Sumini, Effect of the X-ray scattering anisotropy on the diffusion of photons in the frame of the transport theory, Nucl. Instr. and Meth. in Phys. Res. A 280, 212-221 (1989).

51. G.H. Peebles and M.S. Plesset, Transmission of Gamma-rays through large thicknesses of heavy materials, Phys. Rev. 81, 430-440 (1951).

52. I.W. Busbridge, "The mathematics of radiative transfer," Cambridge University Press, Cambridge (1960).

53. J.J. Duderstadt and W.R. Martin, "Transport theory," Wiley, New York (1979).

54. M.M.R. Williams, "Mathematical methods in particle transport theory," Butterworths, London (1971).

55. B. Davison, "Neutron transport theory," Oxford University Press, London (1958).

56. L.L. Carter and E.D. Cashwell, Particle transport simulation with the Monte Carlo method, ERDA Critical Review Series, TID-26607 (1975).

57. E.P. Bertin, "Principles and practice of X-ray spectrometric analysis,", Plenum Press, New York (1975).

58. J. Sherman, The theoretical derivation of fluorescent X-ray intensities from mixtures, Spectrochim. Acta 7, 283-306 (1955).

59. J. Sherman, Simplification of a formula in the correlation of fluorescent X-ray intensities from mixtures, Spectrochim. Acta 11, 466-470 (1959).

60. T. Shiraiwa and N. Fujino, Theoretical calculation of fluorescent X-ray intensities in fluorescent X-ray spectrochemical analysis, Japan. J. Appl. Phys. 5, 886-899 (1966).

61. J.E. Fernández and V.G. Molinari, Theoretical estimation of the fourth-order XRF intensity, in "Advances in X-Ray Analysis" (C.S. Barrett et al., ed.) Vol. 33, pp. 573-580, Plenum Press, New York, (1990).

62. S. Singh, D. Metha, S. Kumar, M.L. Garg, N. Singh, P.C. Mangal and P.N. Trehan, Contribution due to excitation by scattered photons in measurements of L X-ray cross-sections, X-Ray Spectrom. 18, 193-198 (1989).

63. N. Singh, R. Mittal, K.L. Allawadhi and B.S. Sood, Measurement of $L_{l+\alpha}$, L_{β} and L_{γ} X-ray production cross-sections in some rare-earth elements by 10, 18, 26 and 33 keV photons, J. Phys. B 20, 5639-5645 (1987).

64. M.L. Garg, S. Kumar, D. Metha, H.R. Verma, P.C. Mangal and P.N. Trehan, Measurement of photon-induced L X-ray fluorescence cross-sections for Ta, W, Au, Tl and Bi in the 15-60 keV energy range, J. Phys. B 18, 4529-4538 (1985).

65. L. Méray, Simulation of X-ray and gamma-ray scatterings in light matrices, J. Radioanal. Nucl. Chem. Letters 126, 323-334 (1988).

66. L. Méray and E. Házi, Effect of scattered photons on the intensity of X-ray characteristic lines, Acta Phys. Hung. 63, 171-176 (1988).

67. H.D. Keith and T.C. Loomis, Correction for scattering in X-ray fluorescence experiments, X-Ray Spectrom. 7, 225-240 (1978).

68. J.E. Fernández, Rayleigh and Compton scattering contributions to the XRF intensity, X-Ray Spectrom. to be published (1991). 21, 57-68 (1992).

69. "The MACSYMA Reference Manual. Version 4.12," Symbolics, Burlington (1988).

70. W.H. Press, B.P. Flannery, S.A. Teukolsky and W.T. Vetterling, "Numerical Recipes. The Art of Scientific Computing," Cambridge University Press, Cambridge (1986).

71. L.A. McNelles and J.L. Campbell, Analytic approximations to peak shapes produced by Ge(Li) and Si(Li) spectrometers, Nucl. Instr. Meth. 127, 73-81 (1975).

72. H.H. Jorch and J.L. Campbell, On the analytic fitting of full energy peaks from Ge(Li) and Si(Li) photon detectors, Nucl. Instr. Meth. 143, 551-559 (1977).

73. P. Van Espen, H. Nullens and F. Adams, An in-depth study of energy dispersive X-ray spectra, X-Ray Spectrom. 9, 126-133 (1980).

74. B.G. Williams, (ed.) "Compton Scattering: The Investigation of Electron Momentum Distributions," McGraw-Hill, London (1977).

75. M.J. Cooper, Compton scattering and electron momentum determination, Rep. Prog. Phys. 48, 415-481 (1985).

76. W. Schülke, Inelastic X-ray scattering, Nucl. Instr. Meth. in Phys. Res. A 280, 338-348 (1989).

77. J.W.M. Dumond, Multiple scattering in the Compton effect, Phys. Rev. 36, 1685-1701 (1930).

78. B.G. Williams, P. Pattison and M.J. Cooper, The spectral distribution of multiple Compton scattering of X-rays, Phil. Mag. 30, 307-317 (1974).

79. A.C. Tanner and I.R. Epstein, Multiple scattering in the Compton effect. I. Analytic treatment of angular distributions and total scattering probabilities, Phys. Rev. A 13, 335-348 (1976).

80. A.C. Tanner and I.R. Epstein, Multiple scattering in the Compton effect. II. Analytic and numerical treatment of energy profiles, Phys. Rev. A 14, 313-327 (1976).

81. E. Braun-Keller and I.R. Epstein, Multiple scattering in the Compton effect. IV. Operator formalism for nonstationary electrons, Phys. Rev. A 16, 1146-1153 (1977).

82. E. Braun-Keller and I.R. Epstein, Multiple scattering in the Compton effect. V. Bounds on errors associated with multiple-scattering corrections, Phys. Rev. A 16, 1154-1160 (1977).

83. S. Chandrasekhar, The softening of radiation by multiple Compton scattering, Proc. Roy. Soc. A 192, 508-518 (1948).

84. R.C. O'Rourke, Multiple Compton scattering of low energy gamma radiation, Phys. Rev. 85, 881-888 (1952).

85. R.C. O'Rourke, Multiple Compton scattering of low energy gamma radiation, Phys. Rev. 89, 999-1003 (1953).

86. P.J. Brockwell, The multiple Compton scattering of low energy gamma radiation, Phil. Mag. 12, 515-528 (1965).

87. V. Halonen, I.R. Epstein, A.C. Tanner and B.G. Williams, Multiple scattering, in "Compton Scattering: The Investigation of Electron Momentum Distributions" (B.G. Williams, ed.) pp. 79-101, McGraw-Hill, London (1977).

88. J. Felsteiner, P. Pattison and M. Cooper, Effect of multiple scattering on experimental Compton profiles, Phil. Mag. 30, 537-548 (1974).

89. J. Felsteiner and P. Pattison, Monte Carlo study of multiple scattering of photons in Compton profile measurements, Nucl. Instr. Meth. 124, 449-453 (1975).

90. T. Pitkanen, D. Laundy, R.S. Holt and M.J. Cooper, The multiple scattering profile in gamma ray Compton studies, Nucl. Instr. Meth. in Phys. Res. A 251, 536-544 (1986).

91. J.E. Fernández, Rayleigh and Compton double scattering of unpolarised X-rays, Nuclear Engeneering Laboratory Report LIN-1014, University of Bologna (1990). Phys. Rev. A 44, 4232-4248 (1991)

92. R. Sartori and J.E. Fernández, Monte Carlo simulation of multiple scattering effects in energy dispersive X-ray spectrometry, in preparation.

93. J.E. Fernández and M. Sumini, SHAPE: a computer simulation of energy dispersive X-ray spectra, X-Ray Spectrom. to be published (1991). 20, 315-319.

94. S. Holt, X-ray detectors, in "Introduction to Experimental Techniques of High Energy Astrophysics" (H. Ogelman and J.R. Wayland, ed.) NASA Report SP-423, Washington D.C. (1970).

95. G.F. Knoll, "Radiation detection and measurement," John Wiley, New York (1979).

96. S.J.B. Reed and N.G. Ware, Escape peaks and internal fluorescence in X-ray spectra recorded with lithium drifted silicon detectors, J. Phys. E 5, 582-584 (1972).

97. J.L. Campbell, H.H. Jorch and J.A. Thompson, Parametric representation of X-ray detector efficiency curves, Nucl. Instr. Meth. 140, 167-173 (1977).

98. W. Maenhaut and H. Raemdonck, Accurate calibration of a Si(Li) detector for PIXE analysis, Nucl. Instr. and Meth. in Phys. Res. B 1, 123-136 (1984).

99. J.E. Fernández and M. Rubio, Dependence of XRF intensity on the tilt of the propagation plane, X-Ray Spectrom. 18, 281-290 (1989).